

promoting access to White Rose research papers



Universities of Leeds, Sheffield and York
<http://eprints.whiterose.ac.uk/>

This is an author produced version of a paper published in **Physics of Fluids**.

White Rose Research Online URL for this paper:

<http://eprints.whiterose.ac.uk/10137>

Published paper

Caillol, P. (2009) *Absolute and convective instabilities of an inviscid compressible mixing layer: Theory and applications*, *Physics of Fluids*, 21 (10), Art. no.104101

<http://dx.doi.org/10.1063/1.3225142>

Absolute and convective instabilities of an inviscid compressible mixing layer: Theory and applications.

P. Caillol

*Department of Applied Mathematics,
University of Sheffield, Hicks Building,
Hounsfield Road, Sheffield, S3 7RH,
United Kingdom (e-mail: pcaillol@ing-mat.udec.cl)*

(Dated: November 16, 2009)

Abstract

This study aims to examine the effect of compressibility on unbounded and parallel shear flow linear instabilities. This analysis is of interest for industrial, geophysical and astrophysical flows. We focus on the stability of a wavepacket as opposed to previous single-mode stability studies. We consider the notions of absolute and convective instabilities firstly used to describe plasma instabilities. The compressible-flow modal theory predicts instability whatever the Mach number. Spatial and temporal growth rates, and Reynolds stresses nevertheless become strongly reduced at high Mach numbers. The evolution of disturbances is driven by Kelvin-Helmholtz instability that weakens in supersonic flows. We wish to examine the occurrence of absolute instability, necessary for the appearance of turbulent motions in an inviscid and compressible two-dimensional mixing layer at an arbitrary Mach number subject to a three-dimensional disturbance. The mixing layer is defined by a parametric family of mean velocity and temperature profiles. The eigenvalue problem is solved with the help of a spectral method. We ascertain the effects of the distribution of temperature and velocity in the mixing layer on the transition between convective and absolute instabilities. It appears that, in most cases, absolute instability is always possible at high Mach numbers provided that the ratio of slow-stream temperature over fast-stream temperature may be less than a critical maximal value but the temporal growth rate present in the absolutely unstable zone remains small and tends to zero at high Mach numbers. The transition toward a supersonic turbulent régime is therefore unlikely to be possible in the linear theory. Absolute instability can be also present among low-Mach-number coflowing mixing layers provided that this same temperature ratio may be small, but nevertheless, higher than a critical minimal value. Temperature distribution within the mixing layer also has an effect on the growth rate, this diminishes when the slow stream is heated. These results are applied to the dynamics of mixing layers in the interstellar medium and to the dynamics of the heliopause, frontier between the interstellar medium and the solar wind.

Inviscid Instabilities—Compressible—Free-Shear layers—Transition to Turbulence

I. INTRODUCTION

The stability of parallel shear flows is a classic problem of fluid mechanics because it is fundamental to many subjects, ranging from small scales in engineering to synoptic scales in geophysics and meteorology up to astronomical scales in astrophysics. Velocity shear generates a dynamical instability and the most common and fastest one is the Kelvin-Helmholtz (KH) instability which occurs in non-dissipative fluid and plasma shear layers. KH intervenes in many phenomena in fluid dynamics¹⁻³, in space, astrophysical, and laboratory plasmas⁴⁻⁷ when steep velocity gradients emerge. The most relevant examples are the generation of water waves by wind blowing over the surface of the sea water and the solar-wind plasma transport across the terrestrial magnetopause at the interface between the solar wind and the Earth's magnetosphere.

The theory of the compressible-flow stability started from the analytical study of a discontinuous flow generated by a vortex sheet. Landau⁸ proved the stability of this flow for Mach number $M > \sqrt{2}$ with respect to two-dimensional disturbances whereas the basic formulation of the theory of continuous compressible shear flows was given by Lees and Lin⁹. Since then, many new results emerged. A strong interest stemmed about forty years ago from research on hypersonic aircraft engines. The reader can consult the relevant literature in the monograph by Criminale, Jackson and Joslin¹⁰. Some important results deserve anyway to be mentioned here. Blumen¹¹, then Blumen, Drazin & Billings¹² showed that the inviscid and constant-temperature mixing layer whose mean velocity profile is a hyperbolic tangent $U(y) = \tanh(y)$, is temporally unstable with respect to two-dimensional disturbances for any value of M . Three unstable modes exist: one is stationary as $M < 1$ and two are counter-propagating travelling modes as $M > 1$. The latter have growth rates one order of magnitude less than that of the former. Drazin & Davey¹³ showed that, for $M \sim 1$, multiple modes could coexist. Ragab & Wu¹⁴ and Jackson & Grosh¹⁵ examined the spatial instabilities of a free mixing layer with a hyperbolic-tangent-like velocity profile. In their analysis, the mean temperature varies following Crocco relation linking mean velocity and temperature in a compressible boundary layer. They observed two unstable modes and two neutral modes. The so-called first modes, neutral and unstable modes, exist in the subsonic régime when both convective Mach numbers (Mach number defined in the frame moving with the mode) determined with respect to the slow and fast streams are subsonic; they are

located in the domain 1 in the diagram (Mach number, phase speed) in Fig. 1. In that case, the conditions at infinity are an exponential decay of the mode amplitude. Those are called subsonic/subsonic modes and are vortex modes. At high Mach numbers, it is not always possible for modes to have the exponential decay at the two sides of the mixing layer: one or two conditions at infinity are radiative. As M becomes larger than the maximal value M_* for which the exponential decay of neutral modes is possible at both sides, a second mode appears. The first mode as soon as $M \lesssim M_*$ and the second mode are termed slow and fast modes according to the amplitude of their phase speed. The so-called fast mode has the larger phase speed; the neutral fast mode radiates in the slow stream whereas the unstable fast mode may radiate but most often weakly decays in the slow stream and in a more slowly way than in the fast stream. Fast modes are called subsonic/supersonic modes (domain 2 in Fig. 1). The slow mode has an opposite behaviour at infinity, it is a supersonic/subsonic mode (domain 4 in Fig. 1). Slow and fast modes are again vortex modes¹¹. No acoustic modes exist in an unbounded mixing layer either. Acoustic modes appear whenever there is an embedded region of locally supersonic flow relative to the phase speed of the instability wave¹⁶. In both studies^{14,15}, cooling the slow stream results in an increase of the spatial growth rate for any M . An increase of the Mach number leads to a decrease of the temporal growth rate^{12,17}. In the same way, the spatial growth rate¹⁵ may be reduced by a factor of 5 to 10 up to M_* . In unbounded supersonic flows, instability growth rates become smaller and mixing rates lower. At small M , parallel disturbances have the largest growth rates. KH instability weakens as the convective Mach number increases while oblique disturbances become more and more unstable and dominant. Finally, three-dimensional instabilities yield the highest growth rates. As a result, the mixing layer becomes highly three-dimensional. KH instability initiates the formation of coherent structures in a shear layer. Large-scale structures are also observed in supersonic mixing layers. They exist but appear elongated in the streamwise direction and tilted with the high-speed flow without evidence of vortex pairing or other interactions. The transport of vorticity in a compressible and two-dimensional flow is subject to dilatation and baroclinicity. Sandham and Reynolds¹⁷ observed that both related terms in the vorticity equation are negative ahead of the vortex and positive behind, which tends to elongate the coherent structures. These cannot entrain as much fluid as the incompressible near-circular structures. Thus, the most amplified disturbance tends to resist further growth since dilatation and baroclinicity remove vorticity from the location

where vortex roll-up should occur. The disturbance growth rate is reduced by these two compressibility effects which can be considered linear with a very good approximation¹⁷. Moreover, vortices form on the subsonic side of the mixing layer perturbed by supersonic unstable modes, which increases the asymmetry of the motion and subsequently, reduces entrainment. Due to high Mach numbers, upstream and cross-flow communication paths are suppressed. Acoustic interactions between different regions of the shear layer are inhibited, stabilizing the compressible flow¹⁸. Nonlinearity intervenes at a later stage. Initial vortices grow and coalesce as they are advected downstream in a pairing process. Nonlinearity engenders shocks and expansion fans on the supersonic edge of the layer. These shocks are generated inside the shear layer as a result of the coalescence of compression waves. Wall-confined layers are more unstable than free shear layers in supersonic motions; the reflection of acoustic waves from the walls generates a new type of instability: wall-mode instability¹⁹. Shock waves then form from compression waves on the walls. Such waves may engender more intensified turbulent fluctuations and consequently, may lead to mixing enhancement, and are found responsible for the rapid growth of the confined supersonic mixing layer. Shock waves thus form more easily in confined flows. As a result, unconfined mixing layers show weak deviation from linearity²⁰ and we will consider our linear approach still valid at high Mach numbers. Moreover, Ragab & Wu¹⁴ reported that non-parallel effects are negligible and, that the introduction of viscosity has a stabilizing effect at all frequencies but, if the Reynolds number is greater than 1000, the eigenvalue problem can be solved very accurately from inviscid theory, which justifies the assumption that the mean flow will be chosen inviscid and parallel.

We here use again a normal-mode approach but we focus on the spatial development of disturbances while they are advected by their group velocity. We do not examine the instability of a single mode but analyse the behaviour of a wavepacket. We therefore highlight the important distinction between convective and absolute instabilities as initially emphasized in shear flow instabilities by Huerre & Monkewitz²¹. This distinction is clearly dependent upon the reference frame. A flow is said to be *absolutely* unstable if the response to a disturbance in space and time with respect to an observer in a certain frame, is unbounded everywhere for large time. A flow is said to be *convectively* unstable for the same observer in the same frame, if the response decays to zero everywhere; the response is a wavepacket propagating downstream from the source, the waves forming the packet nevertheless grow-

ing. Spatially growing waves can then be only observed if the mixing layer is convectively unstable, otherwise instability develops temporally. This theory therefore yields a refined criterium to predict the location of the transition from a given laminar flow toward a turbulent régime, that lies at the frontier between both instabilities^{21,22}. This picture is clearly an oversimplification of the actual flow development. Transition to turbulence occurs through a sequence of instabilities on a succession of more and more complicated basic flows which are the results of nonlinear equilibria²³. For a better transition prediction, a stability linear analysis should be therefore undertaken on an intermediary equilibrium state, for example Kelvin-Helmholtz billows¹ in the present study. Tracking this transition has a strong interest in industry, since turbulence enhances for instance, mixing in engines, and so, favors combustion. However, growth rates are reduced at high Mach number flows²⁰, which may limit aircraft engine performances. It is therefore important to ask what effect high compression might have on this turbulence threshold. For an opposite reason, the absolute/convective classification of an instability is also an important issue in flow controls. Local forcing of a flow is indeed effective if and only if the motion is convectively unstable. In an absolutely unstable flow, the forcing is rapidly overwhelmed by the in situ growing instabilities. Pavithran & Redekopp²⁴ analysed the convective and absolute instabilities in a free mixing layer when velocity and temperature fields have hyperbolic-tangent-like profiles. The parameters are the Mach number and the ratios of velocities and temperatures of each stream. Jackson & Grosch²⁵ realised a similar study of a boundary layer flow with the same velocity profile but the temperature is linked to the velocity by the Crocco relation. Both papers restricted to the subsonic range. They noticed that the mixing layer became more convectively unstable as the Mach number increased. On the other hand, cooling the slow stream extends the domain of absolute instability. The shear layer can even become absolutely unstable when both streams are coflowing. Terra-Homen & Erdélyi²⁶ determined the absolute/convective instabilities transition by following the development of a Gaussian-spatial-distribution perturbation of the hyperbolic-tangent-like velocity profile through the numerical simulation of the set of complete nonlinear viscous hydrodynamic equations. Temperature was constant, the Mach number was subsonic and the Reynolds number was chosen $R = 10^3$. With these constraints, viscosity had a higher stabilizing effect than compressibility.

Our objective is to track the absolute/convective transition in a free inviscid mixing layer when the Mach number evolves and can attain high supersonic values, to determine for which

velocity and temperature ratios of each stream, this transition exists in spite a KH instability reduction at large Mach numbers. Section 2 formulates the stability problem. Section 3 explicits the spectral method. Section 4 defines the absolute and convective instabilities which occur in an initially perturbed system. Section 5 presents our numerical results. Section 6 applies these results to astrophysical mixing layers, in a first example to the interstellar medium, where two regions with strong differences in density and temperature may interact through mixing layers, and in a second example to the heliopause, where the hot and sparse solar wind encounters the cold and dense interstellar medium. At last, Section 7 offers our conclusions.

II. FORMULATION AND METHOD DESCRIPTION

We consider the linear instability of a two-dimensional compressible mixing layer with zero pressure gradient, which separates two streams of a same gas but of different speeds and temperatures. Temperature and density are related through the perfect-gas law. The flow is unbounded, its direction is following the x -axis, the shear is y -orientated and z is normal to the plane of the flow. We assume that the mean-velocity evolution over the mixing layer is approximated by a hyperbolic tangent. We here assume that viscosity is negligible. The velocity and temperature fields U and T are then uncoupled and we choose for the temperature profile an identical profile to this of the velocity:

$$U = \frac{1}{2} \left[1 + \beta_U + (1 - \beta_U) \tanh(\eta) \right], \quad (1)$$

$$T = \frac{1}{2} \left[1 + \beta_T + (1 - \beta_T) \tanh \left(\frac{\eta}{\eta_T} \right) \right]. \quad (2)$$

The equations of mean motion have been previously turned into their incompressible forms with the help of the Howarth-Dorodnitsyn transformation which introduces a new cross-stream coordinate $\eta = \int_0^y 1/T(y') dy'$, and have as a mean-flow solution the similarity solution given by Lock¹⁵; η_T is the temperature shear layer half-thickness and will be taken equal to one unless indicated otherwise. All quantities are nondimensionalized using the velocity shear layer half-thickness and the magnitudes of the fast-free-stream velocity and temperature, taken to be at $\eta = +\infty$: U_∞ and T_∞ . \hat{M} is the Mach number of the fast stream; β_U is the ratio of the speed of the slow stream to that of the fast stream and β_T is

the equivalent temperature ratio. These ratios satisfy

$$-1 < \beta_U < 1, \quad \beta_T > 0, \quad \text{and} \quad U \rightarrow \beta_U, \quad T \rightarrow \beta_T, \quad \eta \rightarrow -\infty.$$

In the case where viscosity is not negligible, in a boundary layer for example, the mean-temperature profile is determined from the Crocco relation:

$$T = 1 - \frac{1 - \beta_T}{1 - \beta_U}(1 - U) + \frac{1}{2}(\gamma - 1)\hat{M}^2(1 - U)(U - \beta_U). \quad (3)$$

Here, γ is the ratio of specific heats of the gas and is taken constant and equal to $\gamma = 1.4$ for a diatomic gas. We will use this profile for comparison purpose with previous stability studies. Djordjevic and Redekopp²⁷ derived necessary conditions for instability of inviscid, compressible and two-dimensional shear flows through energetical considerations; the local Mach number must be supersonic or

$$U \frac{d}{dy} \left(\frac{1}{T} \frac{dU}{dy} \right) < 0 \quad \text{over at least one zone of the mixing-layer.}$$

The above profiles (1) & (2) indeed always allow for the second quantity being negative over a certain η -range whatever β_U and β_T may be.

These mean fields are perturbed by introducing wave disturbances whose amplitude is function of η ; for example, the pressure perturbation is

$$p = \Pi(\eta) \exp[i(\hat{\alpha}x + \hat{\beta}z - \hat{\omega}t)],$$

with $\hat{\alpha}$ and $\hat{\beta}$ wavenumbers and $\hat{\omega}$ the frequency that are complex.

The equation governing Π is¹⁵

$$\Pi'' - \frac{2U'\Pi'}{U - \hat{c}} - T[(\hat{\alpha}^2 + \hat{\beta}^2)T - \hat{\alpha}^2\hat{M}^2(U - \hat{c})^2]\Pi = 0, \quad (4)$$

where the streamwise wave speed is $\hat{c} = \hat{\omega}/\hat{\alpha}$ and where the prime denotes the derivative with respect to η . Equation (4) is easily turned into an analogous two-dimensional disturbance equation by Squire's transformation

$$\alpha^2 = \hat{\alpha}^2 + \hat{\beta}^2, \quad \hat{\alpha} = \alpha \cos \phi, \quad \hat{\beta} = \alpha \sin \phi,$$

$$\alpha M = \hat{\alpha} \hat{M}, \quad \hat{c} = c, \quad \text{and} \quad \hat{\omega} = \omega \cos \phi.$$

Applying this transformation to (4) yields

$$\Pi'' - \frac{2U'\Pi'}{U - c} - \alpha^2 T [T - M^2(U - c)^2] \Pi = 0. \quad (5)$$

We note that this transformation is not valid for the boundary layer temperature profile because (3) depends on \hat{M} . The boundary conditions for Π are obtained by considering the limiting forms of (5) as $\eta \rightarrow \pm\infty$. The required solutions are exponentials of the form

$$\eta \rightarrow \pm\infty, \quad \Pi \rightarrow \exp(\mp\Omega_{\pm}\eta),$$

$$\text{where } \Omega_{+}^2 = \alpha^2[1 - M^2(1 - c)^2] \quad \text{and} \quad \Omega_{-}^2 = \alpha^2\beta_T[\beta_T - M^2(\beta_U - c)^2]. \quad (6)$$

From now on, \Re and \Im respectively denote the real and imaginary parts of a complex number while the subscripts r and i respectively define the real and imaginary parts of the mode features: frequency, wavenumber and wave speed. The properties of symmetry enable us to restrict the domain of study. Indeed, whatever $\Pi(\alpha, c)$ solution of (5), $\Pi(-\alpha, c)$ and $\Pi^*(\alpha^*, c^*)$ are also solutions, the asterisk indicating complex conjugate. We can therefore restrict the studied (α, c) -domain to $\alpha_r \geq 0$ and $c_i \geq 0$.

We consider weakly unstable oscillations characterizing damping waves escaping from the shear layer. The non-radiation condition for unstable oscillations comes down to $\Re[\Omega_{+}] > 0$ and $\Re[\Omega_{-}] > 0$. A neutral mode with a subsonic convective Mach number M_c such as defined in the Introduction is evanescent but radiates outward with a supersonic convective Mach number. An unstable supersonic- M_c mode may have an exponential decay but this is slower in comparison with subsonic modes.

As the profiles (U, T) have constant ‘‘tails’’, the unbounded-flow problem can come down to a finite-boundary problem in the transverse range $[\eta_{-}, \eta_{+}]$ such as $|U - U(\pm\infty)| \ll 1$ as $|\eta| \geq \max[-\eta_{-}, \eta_{+}]$ (Keller’s boundaries²⁸). The boundary conditions are therefore

$$\left(\frac{d}{d\eta} + \Omega_{+}\right)\Pi(\eta_{+}) = 0 \quad \text{and} \quad \left(\frac{d}{d\eta} - \Omega_{-}\right)\Pi(\eta_{-}) = 0. \quad (7)$$

As the square-root function of a complex number has two branches, one with a positive real part and one with a negative real part, we always consider from now on the first. The forbidden domain or branch cut for Ω_{+} on the complex ω -plane for a fixed α is constituted of the two semi-infinite intervals

$$\omega = \alpha \pm M^{-1}\sqrt{\alpha^2 + a^2}, \quad 0 \leq a^2 \leq \infty,$$

corresponding to waves propagating in a transparent medium. The branch cut for Ω_{-} has a similar expression

$$\omega = \alpha\beta_U \pm \beta_T^{-\frac{1}{2}} M^{-1} \sqrt{\alpha^2\beta_T^2 + b^2}, \quad 0 \leq b^2 \leq \infty.$$

If we factorize Ω by putting $\Omega = \alpha \varpi$, the relation $\Re[\Omega_+] = 0$ is equivalent to

$$\alpha_r \Re[\varpi_+]^2 - \alpha_i M^2 (1 - c_r) c_i = 0. \quad (8)$$

For a temporally unstable mode²⁹, the phase speed is bounded such as $\beta_U < c_r < 1$; we are seeking for solutions that belong to the same c_r -range despite that α is complex. Only in the case where β_T is very small, c_r was found to be slightly less than β_U . We examine the modes that spatially amplify downstream, their spatial growth rate α_i being therefore negative and we assume $c_i \geq 0$ for positive α_r , the condition (8) is then satisfied provided $\Re[\varpi_+] = 0$ and $c_i = 0$ if $\alpha_i \neq 0$. The forbidden phase speed is thus

$$c_+ = 1 - \frac{1}{M}. \quad (9)$$

With $\alpha_i = 0$, neutral modes possess an infinity of branch cuts bounded by c_+ such as $c \leq c_+$. For the slower stream, we have two possibilities; indeed, $\Re[\Omega_-] = 0$ yields the following relation

$$\alpha_r \Re[\varpi_-]^2 - \alpha_i \beta_T M^2 (\beta_U - c_r) c_i = 0. \quad (10)$$

This condition may be satisfied both for $c_i = 0$ and $c_i \neq 0$. In the first case, we have the forbidden phase speed given by

$$c_- = \beta_U + \frac{\beta_T^{\frac{1}{2}}}{M}, \quad (11)$$

and the related neutral-mode branch cuts given by $c \geq c_-$. The branch cuts $c \leq \beta_U - \beta_T^{\frac{1}{2}}/M$ concern very-low-phase-speed modes, so we will omit them from now on. The second case yields the branch cuts

$$c_{2,-} = \beta_U \pm \beta_T^{-\frac{1}{2}} M^{-1} \left[\beta_T^2 + \frac{b^2}{\alpha^2} \right]^{\frac{1}{2}}, \quad (12)$$

where $c_{2,-,i}$ is determined by equation (10) with $\Re[\varpi_-]$ being a function of $c_{2,-,r}$ and $c_{2,-,i}$.

The imaginary wave speed $c_{2,-,i}$ admits two different solutions

$$c_{2,-,i} = \frac{1}{2} (c_{2,-,r} - \beta_U) \left(\frac{\alpha_r}{\alpha_i} - \frac{\alpha_i}{\alpha_r} \right) \pm \left[(c_{2,-,r} - \beta_U)^2 - \frac{\beta_T}{M^2} + \frac{1}{4} (c_{2,-,r} - \beta_U)^2 \left(\frac{\alpha_r}{\alpha_i} - \frac{\alpha_i}{\alpha_r} \right)^2 \right]^{\frac{1}{2}}.$$

The related value of b can be computed through the imaginary part of (12),

$$b^2 = -\beta_T |\alpha|^4 c_{2,-,i} M^2 \frac{c_{2,-,r} - \beta_U}{\alpha_r \alpha_i} \geq 0. \quad (13)$$

These branch cuts have not been until now mentioned in the relevant literature. In the particular subset where $\omega_i = 0$ linked to a spatial instability or a mode giving the transition

from convective instability to absolute instability, the expression of the cut frequency is simplified to

$$\omega_{2,-} = \alpha_r \beta_U \left(1 - \frac{\beta_T}{\beta_U^2 M^2}\right), \quad (14)$$

related to the branch cut parameter

$$b^2 = (\beta_T - \beta_U^2 M^2) \left(\alpha_i^2 \beta_T + \frac{\alpha_r^2 \beta_T^2}{\beta_U^2 M^2}\right)$$

defined on the range: $M \leq \beta_T^{1/2}/|\beta_U|$. For higher M , only the first cut (11) yields an oscillating mode at $-\infty$. After (13) and (14), we note that $c_{2,-,r} < \beta_U$ and $\alpha_r \alpha_i > 0$ if $\beta_U > 0$ and vice-versa. In that subset, the two first branch cuts (9) and (11) refer to neutral modes contrary to the third branch cut (14). Figures 2 show the different branch cuts at fixed values of β_U , β_T and c_i . The curves $c_{2,-,r}$ as a function of M are plotted at constant ratio α_i/α_r . The curve $c_{2,-,r}$ for which $\omega_i = 0$ starts at $c_r = 0$ for $M = 0$, increases with M if $\beta_U < 0$ (decreases if $\beta_U > 0$) and admits a maximum Mach number $M = \beta_T^{1/2}/[|\beta_U|(|\beta_U| + 2c_i)]^{1/2}$ at $c_r = -\text{sgn}[\beta_U]c_i$. Let us find now the location of the unstable modes with respect to the branch cut (14). Let be a spatial mode (α, c) located close to this branch cut such as $c = c_{2,-} + \delta c$; this mode is damped if $\Re[\alpha \varpi_-(c)] > 0$ which comes down to $\Re[\alpha \delta c \partial \varpi_-(c_{2,-})/\partial c] > 0$ for $|\delta c| \ll 1$. Using the second Eq. (6) and $\omega_i(c) = 0$, and after simplifying, we get $\Re[\alpha \varpi_-(c)] = \beta_T \beta_U (\alpha_i M)^2 / (\alpha_r \Re[\varpi_-(c_{2,-})]) \delta c_r$. As a result, if $\beta_U < 0$, then $\delta c_r < 0$, the unstable and damped modes are located below the curve $c_{2,-,r}$ [cf. Figs. 2(a) and 10(a)]; in the same way, their imaginary speed is smaller than $c_{2,-,i}$. If $\beta_U > 0$, these modes are still below $c_{2,-,r}$ but their imaginary speed is higher than $c_{2,-,i}$ [cf. Figs. 2(b) and 12 (only for $M \leq 0.99$)].

The cross-stream group velocity is defined as $v_{g,y} = \partial \omega / \partial \alpha_y$ where the equivalent transverse wavenumber is $\alpha_y = \pm i \Omega_{\pm}$; the y -group velocities on each stream are thus

$$v_{g,y}^+ = \frac{-i \Omega_+}{\alpha M^2 (1 - c)} \quad \text{and} \quad v_{g,y}^- = \frac{-i \Omega_-}{\alpha \beta_T M^2 (c - \beta_U)}.$$

Waves escaping from the shear layer satisfy: $\Re(v_{g,y}^+) > 0$ and $\Re(v_{g,y}^-) < 0$. That yields two other boundary conditions

$$\frac{c_i}{\Re[\varpi_+]} [\Re[\varpi_+]^2 + M^2(1 - c_r)^2] > 0 \quad \text{and} \quad \frac{c_i}{\Re[\varpi_-]} [\Re[\varpi_-]^2 + \beta_T M^2 (c_r - \beta_U)^2] > 0. \quad (15)$$

These conditions are always satisfied provided $c_i \neq 0$; else if $c_i = 0$, three possibilities occur: — if $\Re[\varpi_{\pm}] \neq 0$, no energy goes out of the mixing layer;

— if $\Re[\varpi_+] = 0$, c_r is then less than c_+ and $\Im[\varpi_+]$ must be positive if we wish that $\Re[\Omega_+] = -\alpha_i \Im[\varpi_+]$ be positive. The wave amplitude hence decays at $+\infty$ and energy goes out of the mixing layer at $+\infty$. If $c_r = c_+$, the wave radiates and no energy goes out at $+\infty$.
— If $\Re[\varpi_-] = 0$, c_r is then greater than c_- , $\Im[\varpi_-]$ is taken positive, so that the wave amplitude may decay at $-\infty$ but in this case $\Re[v_{g,y}^-] > 0$, and energy enters the shear layer at $-\infty$. If $c_r = c_-$, the wave radiates and no energy goes in from $-\infty$.

In the subset $\omega_i = 0$, $c_i = 0$ is equivalent to $\alpha_i = 0$, waves radiate at $\pm\infty$ if $\Re[\varpi_{\pm}] = 0$ and $\Im[\varpi_{\pm}]$ can be chosen $\gtrless 0$ so that energy may be exported outward.

In summary, the only modes having a zero imaginary wave speed that must be considered are slow modes expelling energy from the fast stream with

$$c_r < c_-, \quad c_r < c_+;$$

and subsonic/subsonic modes whose energy is trapped in the mixing layer with

$$c_r < c_-, \quad c_r > c_+;$$

among neutral modes, only those being subsonic/subsonic must be considered.

III. THE SPECTRAL METHOD

Let us introduce a new cross-stream coordinate Z such as

$$\frac{\eta}{\eta_+} = \mu Z + (1 - \mu)Z^3, \quad -1 \leq Z \leq 1, \quad (16)$$

with $\eta_- = -\eta_+$ and $0 < \mu < 1$.

Equation (5) rewritten in terms of Z reads

$$\frac{d^2\Pi}{dZ^2} - 2\left[3(1 - \mu)\frac{Z}{E(Z)} + \frac{dU}{dZ}\right]\frac{d\Pi}{dZ} - \alpha^2\eta_+^2 E(Z)^2 T [T - M^2(U - c)^2] \Pi = 0, \quad (17)$$

where $E(Z) = \mu + 3(1 - \mu)Z^2$ and $dU/dZ = (1 - \beta_U)\eta_+/2 E(Z)[1 - \tanh(\eta)^2]$. Its solutions have to satisfy the boundary conditions

$$\left(\frac{d}{dZ} \pm \alpha\eta_+ E(1) \varpi_{\pm}\right)\Pi(\pm 1) = 0. \quad (18)$$

The problem comes down to the search for the eigenvalues $\lambda = \alpha\eta_+ E(1)$ ($\Re(\lambda) \geq 0$) and eigenfunctions Π , the wave speed c being given. For neutral modes, there are singularity and

branch cut related to the equality $U(Z) = c$, which inhibits integrating along the real Z -axis. The profile (1) yields a single critical-layer singularity. In order to avoid such a singularity and large denominators, we integrate along a straight line in the complex z -plane located above or below the singularity, between $z = \eta + i\delta = -\infty + i\delta$ and $+\infty + i\delta$. The mean velocity and temperature then become complex since $\tanh z$ can be written as

$$\frac{\tanh \eta + i \tan \delta}{1 + i \tan \delta \tanh \eta},$$

η being given by (16), and δ varies following the orientation of the viscous sector.

Two independent viscous solutions of the eigenvalue problem, that are solutions of the linearised Navier-Stokes equations, admit an expansion following the small kinematic viscosity ν , for example for the pressure disturbance

$$\Pi^\pm \sim e^{\pm\nu^{-\frac{1}{2}} \int^\eta (i\hat{\alpha}U - i\hat{\omega})^{\frac{1}{2}} d\eta} \left[\Pi^{(0)} + \nu^{\frac{1}{2}} \Pi^{(1)} + \dots \right]. \quad (19)$$

We note that the compressibility assumption does not modify the expression of the exponential factor in (19) compared with the incompressible solutions of the Orr-Sommerfeld equation³⁰. This factor is determined by substituting the leading terms of the expansion (19) into the Navier-Stokes equations and solving a system of two equations for two unknowns u and w , which are the x and z components of the velocity perturbations. The leading term of the y -velocity perturbation v does not intervene because it has a smaller amplitude. If $\Re[(i\hat{\alpha}U - i\hat{\omega})^{\frac{1}{2}}]$ is positive on the entire real η axis, $\Re[\int^\eta (i\hat{\alpha}U - i\hat{\omega})^{\frac{1}{2}} d\eta]$ is then a strictly increasing function on the η axis and Π^\pm are exponentially large at $\eta = \pm\infty$. The general solution of the eigenvalue problem then implies to discard these viscous solutions. Each singularity characterized by its complex location η_c is in fact, on its vicinity, partitioned into three Stokes sectors delimited by Stokes lines defined by $\Re[\int_{\eta_c}^\eta (i\hat{\alpha}U - i\hat{\omega})^{\frac{1}{2}} d\eta] = 0$. If in two sectors, the general solution is given by inviscid solutions, then in one remaining sector, the so-called viscous sector, it is dominated by a viscous solution. The imaginary part $\eta_{c,i}$ being defined modulo π , we then choose $-\pi/2 < \eta_{c,i} < \pi/2$ and δ is expressed by

$$\begin{aligned} \delta &= \eta_{c,i} + \chi(\pi/2 - \eta_{c,i}), & \text{for a viscous sector facing negative } \eta'_i s, \\ \text{or } \delta &= \eta_{c,i} - \chi(\pi/2 + \eta_{c,i}), & \text{for a viscous sector facing positive } \eta'_i s. \end{aligned}$$

A compromise must be done to choose $0 < \chi < 1$. If $|\delta - \eta_{c,i}|$ is too small, resolution must be high to correctly tackle the singularity, if $\tan \delta$ is large with respect to $\tanh \eta$, numerical

oscillations may occur. The viscous sector is defined by³⁰

$$\frac{\pi}{6} - \frac{\arg[\hat{\alpha}U'(\eta_c)]}{3} < \arg(\eta - \eta_c) < \frac{5\pi}{6} - \frac{\arg[\hat{\alpha}U'(\eta_c)]}{3},$$

and never includes the real axis, which allows for an integration contour along a horizontal line. The orientation of the sector is here given by the sign of the real part of $\hat{\alpha}U'(\eta_c)$, that is

$$\hat{\alpha} [c(1 + \beta_U) - c^2 - \beta_U].$$

A Chebyshev collocation method is used to discretize the problem. The collocation points in the interval $[-1, 1]$ are chosen to be the extrema

$$Z_j = \cos \frac{\pi j}{N+1}, \quad j = 0, 1, \dots, N+1,$$

of the $(N+1)$ -st degree Chebyshev polynomial $T_{N+1}(Z)$. If $\mu = 1$, with such collocation points, η clusters around the ends $-\eta_+$ and η_+ . With $\mu \neq 1$, the points are more equally scattered in the range $[-\eta_+, \eta_+]$. We introduce the notation $\Pi_j = \Pi_{N+1}(Z_j)$, $0 \leq j \leq N+1$, Π_{N+1} is the interpolation polynomial of Π of degree $N+1$

$$\Pi_{N+1}(Z) = \frac{1}{2}a_0 + \sum_{n=1}^{N+1} a_n T_n(Z).$$

The discrete version of the differential equation (17) evaluated at each Z_i , $i = 0, \dots, N+1$ leads to $N+2$ relations involving the discretised expressions of Π , $d\Pi/dZ$ and $d^2\Pi/dZ^2$ whose formulae are given in Peyret³¹. By taking the boundary conditions (18) into account, the problem reduces to N linear relations, which in the matricial form can be written as

$$\mathcal{M} \bar{\Pi} = 0, \tag{20}$$

$$\text{with } \mathcal{M} = [\lambda^4 M_0 + \lambda^3 M_1 + \lambda^2 M_2 + \lambda M_3 + M_4] \quad \text{and} \quad \bar{\Pi}^t = [\Pi_1, \Pi_2, \dots, \Pi_N].$$

The companion matrix method³² enables us to obtain a standard eigenvalue system:

$$(A - \lambda I)X = 0,$$

with $X^t = [\lambda^3 \bar{\Pi}, \lambda^2 \bar{\Pi}, \lambda \bar{\Pi}, \bar{\Pi}]$ and A , a $4N \times 4N$ sparse matrix composed of the submatrices M_i , $i = 0, \dots, 4$.

IV. ABSOLUTE AND CONVECTIVE INSTABILITIES

The spectral method described in the preceding section gives the dispersion relation of the eigenvalue problem, that are the roots α of $\mathcal{D}(\alpha, c) = 0$, c being given. We are now going to focus on the double α -roots (α_0, ω_0) of the equation $D(\alpha, \omega) = \mathcal{D}(\alpha, \omega/\alpha) = 0$.

The general evolution for an initial perturbation can be formally expressed by a Laplace-Fourier integral

$$q(x, y, t) = \int_{i\sigma-\infty}^{i\sigma+\infty} e^{-i\omega t} d\omega \int_{-\infty}^{\infty} \frac{F(\alpha, \omega, y)}{D(\alpha, \omega)} e^{i\alpha x} d\alpha \quad (21)$$

where σ is larger than the largest growth rate of any mode for real α . F is an analytic function depending on external perturbations like initial conditions. The line along which we integrate in the complex ω -plane is the Laplace or Bromwich contour. In the α -plane, the integration path is the Fourier contour. The initial-value problem is well-posed. Indeed, the temporal growth rate of an unstable mode in a two-dimensional inviscid compressible shear flow is bounded²⁹ by

$$\omega_i \leq \frac{1}{2} |U'|_{\max}. \quad (22)$$

Double α -roots of the dispersion relation D determine the large-time behaviour of the initial-value problem. The behaviour of the disturbance when $t \rightarrow \infty$ is given by the double root (α_0, ω_0) that has the largest imaginary part⁶ of the frequency ω_0 :

$$\Pi \sim \frac{1}{\sqrt{t}} e^{-i\omega_0 t} e^{i\alpha_0 x}.$$

These roots satisfy the equations

$$D = \text{Det}[\mathcal{M}(\alpha_0, \omega_0/\alpha_0)] = 0 \quad \text{and} \quad \frac{\partial D}{\partial \alpha}(\alpha_0, \omega_0) = 0.$$

The second equation is equivalent to $\partial\omega/\partial\alpha = 0$. The related root α_0 is a saddle-point in the complex α -plane, meeting point of upstream and downstream branches and ω_0 is a branch point in the complex ω -plane. The instability is absolute if the branch point is in the upper-half plane, or convective if it is in the lower-half plane, provided that both the α -branches are generated on opposite sides of the real α axis when ω_i evolves from the Bromwich contour $\omega_i = \sigma$ up to $\omega_i = \omega_{0,i}$ and such as $\omega_r = \omega_{0,r}$. This is the so-called pinching condition that we have verified for each M_c -régime: subsonic, transonic and hypersonic. To do so, we have used a Runge-Kutta scheme integration of Eq. (5) because we need have ω as independent variable and α as dependent variable, and c expressed as ω/α .

We now explain the procedure for evaluating the double roots of our dispersion relation. In a reference frame moving with the constant speed V , the Doppler-shifted frequency becomes $\tilde{\omega} = \omega - \alpha V$ and a double root has this frequency which satisfies: $\partial\tilde{\omega}/\partial\alpha(\alpha_0) = 0$. A standard algorithm consists in determining $\alpha_{0,r}$ for a given α_i by solving $\partial\omega_i/\partial\alpha_r(\alpha_{0,r}, \alpha_i) = 0$, next one deduces $V = \partial\omega_r/\partial\alpha_r(\alpha_{0,r}, \alpha_i)$. The double-root in the laboratory frame is found out while incrementing α_i up to $\alpha_{0,i}$ when $V = 0$. The approach must be here modified. Indeed, c is now the independent variable and α is the dependent variable. The reference frame saddle-point is hence determined while varying c_r and fixing c_i by computing the root c_r of

$$c_i \left[\left(\frac{\partial\alpha_r}{\partial c_r} \right)^2 + \left(\frac{\partial\alpha_i}{\partial c_r} \right)^2 \right] + \alpha_i \frac{\partial\alpha_r}{\partial c_r} - \alpha_r \frac{\partial\alpha_i}{\partial c_r} = 0. \quad (23)$$

The reference frame speed V is then given by

$$V = c_r + \frac{c_i \frac{\partial\alpha_r}{\partial c_r} + \alpha_i}{\frac{\partial\alpha_i}{\partial c_r}}. \quad (24)$$

All partial derivatives are calculated at constant c_i by the finite-difference approximation. According to Briggs-Bers criterion, the moving frame is absolutely unstable if $\tilde{\omega}_i > 0$ and convectively unstable if $\tilde{\omega}_i < 0$. We note that using c as independent variable is in fact more convenient than using α . Indeed, after the semi-circle theorem valid for two-dimensional compressible flows^{11,29}, temporally unstable modes ($c_i > 0$) have their wave speed which is bounded in the complex plane and located within a semi-circle centred at $(U_{\min} + U_{\max})/2$ and of radius $(U_{\max} - U_{\min})/2$. Though we here consider complex-frequency-and-wavenumber modes, this result revealed to be mostly true for the ranges of parameters considered and made our eigenvalue search easier.

V. NUMERICAL RESULTS

The spectral method was tested by solving the eigenvalue problem with a second method, a fourth-order Runge-Kutta scheme straightforward integration of (5) after a Ricatti transformation on the function $\mathcal{P} = \Pi'/\Pi$ and a change of variable $\eta \rightarrow \Lambda = \tanh(\eta)$ in the same way as Blumen¹¹. Figure 3(a) shows the double roots of the dispersion relation giving the transition from convective to absolute instabilities for $\beta_T = 0.5$ (M varying from 0 to 1) and $\beta_T = 1$ (M varying from 0 to 5). These double roots, denoted from now on ACT, have

already been computed by Jackson and Grosch²⁵ in the subsonic range for the boundary layer temperature profile (3). We have computed them both with the spectral method and the Runge-Kutta scheme. The agreement is excellent. We notice that a strong departure between the transitions with profiles (2) and (3) occurs as soon as $-\beta_U$ starts to decrease and this difference increases with M . The boundary layer experiences an earlier transition to absolute instability than the mixing layer in the supersonic range; the asymptotic behaviours as $M \gg 1$ are respectively $-\beta_U = O(M^{-2})$ and $-\beta_U = O(M^{-1})$.

The resolution in number N of polynomials depends on which way the eigenfunctions behave at $\eta = \infty$. As a result, let us have a look at the asymptotic behaviour of the coefficients Ω^\pm related to the ACT double roots as $M \rightarrow \infty$. These behaviours have been obtained by least-square fits on α and c :

$$\begin{aligned}\Re[\Omega_+] &\sim (\beta_T M)^{-1}, & \Re[\Omega_-] &\sim (\beta_T M^9)^{-\frac{1}{4}}, \\ \Im[\Omega_+] &\sim \beta_T^{-1}, & \text{and } \Im[\Omega_-] &\sim (\beta_T M^7)^{-\frac{1}{4}}.\end{aligned}\tag{25}$$

The exponential decay decreases with M , N must therefore increase with M . If β_T is small, oscillations at $\pm\infty$ have a much higher frequency, so N must increase as β_T decreases. On the contrary, the smallness of β_T plays in favour of the exponential decay at $\pm\infty$. As a result, for small and large β_T 's, a high resolution in N is necessary. In those cases, the Runge-Kutta scheme does not manage to follow the steep oscillations of the eigenmode at infinity, how small the integration step may be chosen. The spectral method is therefore required at $\beta_T \neq O(1)$ or $M \gg 1$.

Figures 4 show isocontour levels $\omega_i = \text{const}$ in the α -plane at the absolute instability threshold, and obtained by the Runge-Kutta scheme. As ω_i tends to zero, each pair of sets of contours $\omega_i > 0$ and $\omega_i < 0$ pinches at the saddle point α_0 . As $\omega_i > 0$ increases, the related pair recedes into their respective half-planes $\alpha_i > 0$ (branch α^+) and $\alpha_i < 0$ (branch α^-). We note that the contours are not as accurate at $M = 3$ as at $M = 0.5$, which is an illustration of the above remark concerning the Runge-Kutta scheme. For the mixing-layer velocity profiles studied here, there are three branches of spatial eigenvalues²¹: $\alpha_1^+(\omega)$, $\alpha_1^-(\omega)$ and $\alpha_2^+(\omega)$. The two first correspond to the first mode mentioned in the Introduction which has two counterparts: upstream and downstream, and the third corresponds to the second mode. The latter appears as soon as $M = M_*$. Only α_1^+/α_1^- and α_2^+/α_1^- pinchings are relevant. Once a double root satisfying (23) and (24) is detected in our computation, we

must check first, that this mode is the meeting point of upstream and downstream modes, second that it is the mode with the largest Doppler-shifted growth rate $\gamma = \omega_i - \alpha_i V$. As we focus on transition modes with $\omega_i = 0$ in the laboratory frame $V = 0$, we need check that if one pinching mode was obtained for a certain value of $-\beta_U$ with $\omega_i = 0$ and $V = 0$, then for a smaller value of $-\beta_U$, one does not observe a similar second pinching. Figure 5(a) shows γ as a function of V for the $M = 2$ -mixing layer. The left hump corresponds to the first mode and the right hump to the second mode. In the isothermal mixing layer, for $\beta_U = -0.3116$ ($M/M_* \simeq 1.31$) related to the absolute-instability threshold, $\gamma = 0$ at $V = 0$. For $\beta_U = -0.1$ ($M/M_* = 1.1$), $\gamma < 0$ at $V = 0$, the motion is convectively unstable in the laboratory frame. As $-\beta_U$ decreases, both humps come over and merge at $\beta_U = 0$ ($M = M_*$). For $\beta_U \geq 0$, there exists a single hump related to the first mode. In practice, the wavepacket thus parts into two packets, and the slower packet will give the convective or absolute nature of the instability. The slow mode/slow hump relation is easily checked as the phase speed uniformly increases with the real group velocity V (cf. Fig. 5b). The unbounded-mixing-layer transition from a convective instability toward an absolute instability is thus given by the pinching of two slow modes which are two first modes. We observe furthermore that the phase speed c_r does not strongly vary with β_T and β_U and does not depart too much from the propagation speed of unstable modes within the wavepacket. The real group velocity V is all the smaller so since M/M_* is large. For $\beta_T > 1$, the faster hump possesses a higher maximum than the slower and still characterizes the second modes in spite of the fact that fast-mode spatial growth rates are always smaller than slow-mode ones as we will check later on. For $\beta_T < 1$, the slower hump possesses the higher maximum. For $\beta_T = 0.02$, this maximum attains $\gamma_{max} \simeq 0.103$ which is more than 2000 times larger than the fast-mode maximum and nearly 10 times the slow-mode maximum at $\beta_T = 0.5$. The maximum growth rate γ_{max} increases as β_T decreases but, γ_{max} does not nevertheless tend to infinity as β_T tends to zero. The curves γ for $\beta_T = 0.02$ ($M/M_* = 1.75$), $\beta_T = 0.5$ ($M/M_* = 1.39$) and $\beta_T = 2$ ($M/M_* = 1.24$) are not complete. The gap between the smaller and larger values of V corresponds to the domain where no decaying modes exist; $\Re[\Omega_+]$ becomes negative in the decreasing part of the left hump and $\Re[\Omega_-]$ becomes negative in the increasing part of the right hump.

Caillol and Ruderman³³ showed that the absolute/convective instability diagram is qualitatively divided into two domains, one for the Mach number less than a critical value M_{cr}

and the second for $M > M_{cr}$. Increasing M in the first domain makes the mixing layer less absolutely unstable whereas an inverse behaviour occurs in the second one. We assume that the critical Mach number M_{cr} is related to M_* , the Mach number for which the branch cuts (9) and (11) from both streams intersect: $c_+(M_*) = c_-(M_*)$ (cf. Fig. 1). Indeed, after Jackson & Grosch¹⁵, this Mach number corresponds to a minimum of the maximum growth rate for spatially growing modes and it is expressed by

$$M_* = \frac{1 + \beta_T^{\frac{1}{2}}}{1 - \beta_U}.$$

That number corresponds to the change of modes, from a subsonic/subsonic mode to a slow supersonic/subsonic mode, from the domain 1 to 4 passing through the curve c_+ in Fig. 1. We then define a new convective Mach number by

$$M_c = \frac{M}{M_*}.$$

This number is of interest in experiments. Indeed, it enables one to diminish the number of parameters describing instability. Normalized-growth-rate curves with different β_T 's collapse onto a single curve³⁴ for $M_c < 1$.

We now describe the results of our computations. Figure 3(b) shows the values of $-\beta_U$ for the ACT branch point as a function of M_c for different values of β_T . Increasing the Mach number for $M \lesssim M_*$ makes the amount of backflow needed to cause absolute instability higher, but as soon as $M \gtrsim M_*$, the tendency is inversed at such a point that the minimum ACT velocity ratio is given for $\beta_T > 0.1$ at the largest Mach number that the mixing layer can attain; its asymptotic value is $\beta_U = 0$ as $M \rightarrow \infty$. The values of M_c related to the maxima of $-\beta_U$ are for $\beta_T = 0.5, 1$ and 2 quite close: $1.115, 1.008$ and 0.910 , which makes M_c a good parameter. The asymptotic value $\beta_U = 0$ corresponds to the most unstable mixing layer profile when M tends to infinity. Indeed, the ACT double root asymptotes at high M the double root possessing the highest imaginary part of the frequency; the absolutely unstable zone is thus shrinking to zero. Figures (6) show these double roots for $\beta_T = 1$ as a function of the convective Mach number. The maximum-shear state at $\beta_U = -1$ only yields the highest temporal growth rate in the subsonic régime. The amount of backflow necessary to cause the highest instability decreases rapidly with M . Around $M \simeq M_*$, the curves $-\beta_U$ and ω_i experience a discontinuity while passing from a subsonic vortex mode to a slow vortex mode, such a discontinuity is observed in the same passage of the maximum

spatial growth rate¹⁵. The increase of the absolute-instability zone as soon as $M \geq M_*$ is linked to the $\beta_{U,ACT}$ curve evolution which cannot cross the maximum- ω_i curve and must asymptote it by inferior values. By interpolating the values of β_U at high Mach numbers, we find $-\beta_U \sim \beta_T^{1/2}/M$ for the mixing-layer temperature profile (cf. Fig. 10 b). The constant of proportionality is evaluated with an accuracy around 90% for $M = 7$.

The double root that is considered here is the first mode, since it exists whatever M unlike the second mode which appears at $M = M_*$. It possesses the larger spatial growth rate and becomes a slow mode as it comes into the domain 4 in Fig. 1. The slow or fast nature of the mode is function of β_U and β_T . For negative or slightly positive β_U as has been encountered here, the ACT double root is always the slow and first mode, but with $\beta_U = 0$ and the temperature profile (3) as in Jackson and Grosch¹⁵ and in Ragab and Wu¹⁴, the maximum-growth rate first mode becomes fast as $\beta_T > 1$, and the second mode is the most spatially unstable as $\beta_T < 1$. A supersonic mode is termed respectively slow or fast if $c_r < c_-$ or $c_r > c_+$ when $M \gtrsim M_*$; a typical example is illustrated in Figs. 7 where spatial modes are displayed, (a) gives the phase speed plotted with respect to the frequency ω_r for $M_c = 1.01$ and $\beta_T = 1$ at the absolute-instability threshold, the first mode being then pinched. The first mode has its phase speed c_r smaller than this of the fast mode. Their phase speeds coincide at $\omega_r = 0$ and $\alpha = 0$ and are equal to c_- . The meeting point of the c_r -branches where a cusp occurs³⁵ is a ACT mode. The c_r -branch corresponding to α_1^+ is the upper branch. The phase speed range on the branch α_1^+ lies between 0.140 and 0.333. At $M_c = 1.88$, this range is reduced to 0.049 – 0.079. As Jackson and Grosch¹⁵ noticed, unstable modes have a weak dispersion. In the $(\omega_r, -\alpha_i)$ graph, the absolute frequency of the maximum-spatial-growth rate mode on the lower branch α_1^+ is smaller than the slow-neutral-mode frequency ω_N . This maximum becomes the ACT mode when it presents a cusp while β_U is varied. Figures 7(b) and 8(b) show that the fast-mode growth rate is not negligible when $M \sim M_*$ and when β_T is of order one; on the contrary, when $M_c \simeq 1.88$, the fast-mode growth rate is very small. For small values of β_T , the fast mode also has very small growth rates at $M_c \sim 1$, as Fig. 9 shows at $\beta_T = 0.02$ and $\beta_T = 0.1$. Moreover, its domain of existence is strongly reduced due to the condition: $\Re[\Omega_-] > 0$.

The ACT-mode phase speed is smaller than the slow-neutral-mode phase speed. As $M \rightarrow \infty$, both phase speeds tend to c_- . In Fig. 10(a) for $\beta_T = 1$, the ACT and neutral modes become quasi-identical for $M_c \geq 2$, which justifies the use of the integration in the

complex plane. The slow-neutral-mode curve experiences a sharp discontinuity while passing on the curve c_+ , that corresponds to the passage from a regular mode to a singular mode. The discontinuity of the ACT mode is much weaker, it is a small trough. The slow neutral mode radiates at $\eta = +\infty$ and is evanescent at $-\infty$. The slow unstable ACT mode decays both at $\pm\infty$ but with more difficulty in the fast stream than in the slow stream as the leading-order imaginary parts of Ω_- and Ω_+ confirm in (25) in the case where $M \rightarrow \infty$.

The domain of absolute instability is extended at any Mach number by cooling the slow stream. This result may be linked to the increase of the spatial growth rate whatever M as β_T is decreased¹⁵ and is due to the effect of the baroclinic torque arising from base-flow temperature gradients and from pressure perturbations $\mathbf{\Gamma} = -(\nabla T \times \nabla p')$. When the baroclinic torque is cancelled from the perturbation equations, the convective-absolute transition in a compressible axisymmetric wake³⁶ for instance, is nearly independent of β_T . As $\beta_T \lesssim 0.1$, the ACT velocity ratio β_U becomes positive for small M , the earliest AC transition is therefore near the incompressible state. For β_T and M_c sufficiently small, the shear layer may become absolutely unstable even when the streams are coflowing. The velocity ratio β_U becomes positive for $\beta_T = 0.1$ as $M_c < 0.608$ and reaches values of order 10^{-3} and for $\beta_T = 0.02$ as $M_c < 1.752$, β_U attains values of order 10^{-2} . However, there does not always exist ACT modes at small β_T 's and at subsonic régime. Indeed, the condition $\Re[\Omega_-] > 0$ is no longer satisfied owing to the high values of $c_{i,ACT}$ in that zone: $c_i \gg |\beta_U - c_r|$. The graph in Fig. 1 is made by assuming c_i negligible in front of $1 - c_r$ and $|\beta_U - c_r|$ and is therefore inexact in the small- β_T domain. This non-permitted domain had not been discovered previously because larger values of β_T had been examined; Jackson and Grosch²⁵ reported the stiffness of the eigenvalue computation at small β_T and restricted their study to $\beta_T \geq 0.15$. The latter domain is bounded by the branch cut (14). The curve of the critical minimum temperature ratio β_T has been plotted in Fig. 11(a) by seeking for the smallest β_T for which it is still possible to find a ACT mode, at each M , possessing a positive $\Re[\Omega_-]$. We have superimposed to these numerical values the value of β_T given by Eq. 14, β_U , α and c taking the numerical values of the ACT mode. $\beta_{T,min}$ slowly varies over the M -range $[0, 0.9]$, then it decreases sharply and at $M = 0.99$, $\beta_{T,min} = 0$. The numerical values of α on the branch cut do not converge rapidly as $\beta_T \rightarrow \beta_{T,min}$, these values are all the more inaccurate at small M so since $\alpha_r \rightarrow 0$ for $M \rightarrow 0$. Figure 12 shows that the existence of ACT modes at $\beta_T = 0.02$ is strongly reduced in the domain 1 of the graph in Fig. 1. The curve $c_{2,-,r}$

meets the $c_{r,ACT}$ curve at $M \simeq 0.978$. On the other hand, heating the slow stream decreases the domain of absolute instability. As soon as $\beta_T > 4.662$, absolute instability vanishes first at $M = 1.1$, ($M_c = 0.696$) (cf. Fig. 11 a). For $\beta_T > 5.453$, absolute instability ceases to exist in the subsonic range from $M = 0$ up to $M \sim 1.74$ ($M_c \sim 1.04$). Figure 11 (b) displays $-\beta_U$ as a function of M_c for $\eta_T = 1$ and $\eta_T = 0.1$ at $\beta_T = 2$. When temperature evolves 10 times more rapidly over the mixing layer with respect to velocity, the passage to absolute instability then occurs earlier. The departure vanishes at high M . The earliest passage is therefore given by a true temperature discontinuity.

Figure 13(a) shows the ACT absolute frequency ω_r as a function of M_c . When $\beta_T = O(1)$, this decreases with M_c . When β_T is small, ω_r has a maximum at a certain M_c that is all the larger so since β_T is small. The hotter the slow stream is, the smaller the ACT frequency is. The frequency decays rapidly toward zero at high Mach number as $\omega_r = O\left(\beta_T^{-1} M^{-7/2}\right)$. The branch cuts c_- and c_+ are not intersected by the ACT double roots because $c_{i,ACT} = 0$ is only reached asymptotically. In Fig. 13(b), we have represented the curves ω_r , $\alpha_r c_-$ and $\omega_{2,-}$ as functions of M_c for $\beta_T = 0.5$ and 2. The frequencies $\alpha_r c_-$ and $\omega_{2,-}$ always have higher values. ω_r approaches asymptotically $\alpha_r c_-$ with $\omega_r \leq \alpha_r c_-$. The branch cut (14) has a twice larger frequency than $\alpha_r c_-$ for $M \rightarrow \infty$:

$$\omega_{2,-} \sim 2\alpha_r \left(\beta_U + \frac{\beta_T^{\frac{1}{2}}}{M} \right) = 2\alpha_r c_-.$$

Figures 14 display the absolute wavenumber as a function of M_c , its evolution is very similar to that of the absolute frequency; α_r reaches a maximum for $\beta_T \lesssim 1$ strongly increasing when β_T decreases; α_r reaches a maximum value of 2.539 at $M_c = 1.412$ for $\beta_T = 0.1$ and this value becomes 12.569 at $M_c = 3.085$ for $\beta_T = 0.02$. As β_T is divided by 5, the maximum wavenumber is multiplied roughly by 5 which yields a viscous dissipation enhanced by 25. We hence expect the high instability of the cooled-slow-stream mixing layers to be attenuated by viscosity and thermal conduction. In the supersonic range, α_r diminishes slowly toward zero in the following way: $\alpha_r = O(\beta_T^{-1} M^{-1})$. Figures 15 give the spatial growth rate of the ACT branch point. In the subsonic range, it decreases slightly for order-one β_T and then more rapidly in the supersonic range. At high M , α_i tends to zero such as: $-\alpha_i = O(\beta_T^{-1} M^{-2})$. The spatial instability is all the higher since the slow stream is cooled; $-\alpha_i$ possesses a maximum for very small values of β_T . At $\beta_T = 0.1$, we observe a small bump at $M_c \sim 1$; at $\beta_T = 0.02$, this is substituted by a true maximum at $M_c \sim 2$ with $-\alpha_i = 12.147$. Figures

16(a) and (b) show the real and imaginary wave speed evolutions. They are very similar. The cooler the slow stream is, the smaller the wave speed is at subsonic and supersonic régimes. The decay toward zero at high Mach number does not however depend on β_T , indeed for $M \gg 1$, $c_r = O(M^{-\frac{5}{2}})$ and $c_i = O(M^{-3})$. For very small β_T , c_r tends to zero at small M_c .

The effects of a three-dimensional perturbation are reported on Figs. 17; $-\beta_U$ is plotted as a function of the primitive Mach number $\hat{M} = M/\cos\phi$ for $\phi = 0, 30^\circ, 45^\circ, 60^\circ$ and 75° . Inclination tends to delay the evolution of β_U with respect to \hat{M} . Consequently, for nearly transverse cases, \hat{M} is mostly located in the first domain mentioned earlier since it is practically always less than $M_{cr}/\cos\phi$. Compressibility thus has a stabilizing effect, and the higher ϕ is, the larger the domain of absolute instability is. The spatial growth rate $-\alpha_i$ of a oblique ACT mode seen by an observer moving with the mode along its wavenumber direction decreases more slowly than this of a parallel mode. As a result, an oblique mode is all the more spatially unstable so since ϕ is large. The absolute wavenumber α_r behaves in the same way.

All these results are related to hyperbolic-tangent-like mean-velocity-and-temperature profiles. The choice of the latter comes from the good fits that such profiles have with experimental data in the self-similarity zone³⁷. Those profiles are therefore employed predominantly in numerical and analytical stability studies. The Error function is also often employed because it is an approximate self-similar solution of the mean-flow equations³⁸. Qualitatively, identical behaviours are observed for mixing layers described by both functions when they perturbed by wavelike disturbances³⁹. We have compared in Fig. 18 (b) the ACT velocity ratio $-\beta_U$ at $\beta_T = 0.1$ and $\beta_T = 2$ for both functions. The Error-function mixing layer leads to an earlier absolute instability as the related shear-layer thickness is slightly smaller than the Tanh shear layer's at identical β_U (cf. Fig. 18 a) for any $-1 \leq \beta_U \leq 1$. The vorticity thickness²⁰ for the former layer is $\sqrt{\pi}/2$ smaller than this of the latter. The asymptotic behaviours of α , c and ω are identical as $M \rightarrow \infty$ for both profiles. We assume that all profiles evolving exponentially outside the mixing layer qualitatively experience similar absolute and convective transitions bounded by limiting values for β_T as shown in the Fig. 11 in the case of the Tanh profile. The instability transitions for other profiles, as algebraically decaying at infinity, are beyond the scope of the paper as the numerical procedure presented here is not valid and are of small interest since those profiles are not mentioned

in the literature.

VI. APPLICATIONS

The interstellar medium (ISM) is a very complex entity. ISM shows regions of distinct physical conditions, which range from cold and molecular, to hot and ionized. Begelman and Fabian⁴⁰ realized that the interfaces between hot and warm media might well be dominated by “turbulent mixing layers”. Though ISM is embedded in a dynamical magnetic field, we neglect it as Esquivel et al.⁴¹ did in a part of their simulations when they modelled turbulent mixing at the boundary between hot and warm materials in the ISM. They indeed showed that its effects were found to be minimum at earliest times corresponding to the linear stage of the perturbation evolution. In this section, we model the early evolution of this perturbed boundary by assimilating it to the mixing layer described in the previous sections. The fluid is a gas constituted by protons and electrons. Our model has however a weakness; it does not take the radiative cooling into account. The turbulent-mixing-layer model⁴⁰ includes radiative cooling because, if energy were conserved, the mixing layer would grow up indefinitely by constant production of turbulence at the interface of both plasmas. A steady state then occurs subsequently due to a balance between a turbulent heat flux into the mixing layer and radiative cooling. The latter makes the KH instability developing faster⁴¹. Typical ISM conditions⁴¹ are $T_{\text{hot}} \sim 5 \cdot 10^5 \text{ K}$ and $T_{\text{warm}} \sim 10^4 \text{ K}$ ($\beta_T \sim 0.02$), with a velocity V_{hot} in the hot medium and no mean motion in the warm medium ($\beta_U \sim 0$). The thickness of the shear layer is of the order of a parsec ($\simeq 30.9 \cdot 10^{12} \text{ km}$), $L \sim 1 \text{ pc}$ and hydrogen number densities are $n_{\text{hot}} \sim 10^{-4} \text{ cm}^{-3}$ and $n_{\text{warm}} \sim 5 \cdot 10^{-3} \text{ cm}^{-3}$. The ratio of specific heats of this monoatomic-hydrogen gas is $\gamma = 5/3$. The Mach number in the hot medium is then $M = V_{\text{hot}}/c_s$, the sound speed being $c_s = (2\gamma R/M_p T)^{\frac{1}{2}}$ with R the universal gas constant and M_p the proton molar mass. Table I gives the state of the mixing layer for different values of V_{hot} . The AC transition at $\beta_U = 0$ is located at $M_c \sim 1.75$ corresponding to a velocity of the fast-stream gas $V_{\text{hot}} = 240 \text{ km s}^{-1}$. For a velocity greater than 240 km s^{-1} , the speed is so large over most of the mixing layer than the disturbance is carried away and does not have enough time to develop anywhere, so the mixing layer in that case is convectively unstable. Perturbations grow spatially with the mode which possesses the largest spatial growth rate. For $V_{\text{hot}} < 240 \text{ km s}^{-1}$, the mixing

layer is absolutely unstable and disturbance evolves with the mode which is the slow double root of the dispersion relation. Its imaginary frequency yields its e-folding time τ , and its real wavenumber, its spatial period L . τ does not decrease uniformly when M_c decreases. L attains very large scales for small M_c . For $V_{\text{hot}} > 240 \text{ km s}^{-1}$, the e-folding length L_e is very small; as a result, strongly and spatially amplifying waves may exist in the mixing layer. This amplifying effect is due to the strong temperature difference between both media and is caused by the baroclinic torque. The turbulent-mixing-layer computations⁴¹ show that only small-scale modes are present in the first linear stage of disturbance evolution and the temporal growth rates remain low for all simulations. The e-folding time of the absolutely unstable mixing-layer evolution is very small in the Table I compared to the time of order Mega years around which the mixing layer reaches a steady state when nonlinearities saturate the KH instability⁴¹. The modelled mixing layers then belong to the weakly-absolute-instability régime that exists for $200 \text{ km/s} < V_{\text{hot}} < 240 \text{ km/s}$ (cf. Table I) but later on, secondary instability causes the large-scale modes to prevail.

A second application of this study is the solar-wind interaction with the interstellar medium, interaction which yields two shocks: the bow shock which is the shock through which the IS wind passes and is decelerated by the solar wind and the heliospheric shock through which the solar wind passes and is decelerated by the IS wind (cf. Fig. 19). Both compressed IS and solar winds interact within a mixing layer called the heliopause. We suppose that the disturbance wavelength is smaller than the curvature of the heliopause radius; the flow along the heliopause can be then considered as parallel. The IS wind, a gas of temperature T_{IS} and proton density n_{IS} moves with a supersonic speed V_{IS} with respect to the Sun. As a discontinuity in density and velocity, Rayleigh-Taylor and Kelvin-Helmholtz instabilities may occur along the heliopause. The second instability is expected to be more efficient on the flanks, where the shear flow is more pronounced, away from the stagnation point. As the gravity force is sunward, the dynamics of the heliopause around the stagnation point is very similar to this of two still layers, the upper layer being heavier than the lower one. The Rayleigh-Taylor instability may thus exist near the “nose” point where the difference between the plasma densities on both sides of the interface is the largest⁴². At low polar angle $\theta < 30^\circ$, Rayleigh-Taylor instabilities are likely to occur but for larger angles, Kelvin-Helmholtz instabilities develop⁴³. If we choose numerical values from the recent observations

by Ulysses⁴⁴, $n_{IS} = 0.06 \text{ cm}^{-3}$, $T_{IS} = 6500 \text{ K}$ and $V_{IS} = 26.4 \text{ km s}^{-1}$, and for the solar wind around the Earth $n_{SW} = 8 \text{ cm}^{-3}$, $T_{SW} = 2 \cdot 10^5 \text{ K}$ and $V_{SW} = 445 \text{ km s}^{-1}$, yielding the location of the termination shock around 100 AU away from the Sun. The IS wind contains H neutral atoms, but we neglect their effects on the heliopause dynamics, effects which intervene while the charge exchange of H atoms with IS gas protons occurs. The modal equation (4) would be much more complex if we took the presence of H neutral atoms in the plasma into account. With this assumption, Baranov⁴⁵ gives tangential velocities and pressures along the heliopause as functions of θ . For θ varying from 30° to 90° , β_U and β_T are practically constant, $\beta_U \sim 0.081$ (cf. Table II for β_T). On the contrary, the convective Mach number undergoes a higher variation, increasing with θ . We are in the cooled-slow-stream and coflowing-layer régime where absolute instability may be possible as $\beta_T < 0.1$. We are still however in the convectively unstable régime because $\beta_U > \beta_{U,ACT} \sim 10^{-2}$. We notice that this zone needs a more complex model since we have seen that viscous and thermal dampings were not negligible owing to the high values of the ACT absolute wavenumber. The solar rotation generates forced perturbations on the heliopause of period 27 days, which corresponds to a frequency of $4.3 \times 10^{-7} \text{ s}^{-1}$. Assuming a heliopause thickness of 20 AU , we can deduce the dimensionless forcing frequency for each polar angle, at $\theta = 30^\circ$, $\omega = 7.14$, $\theta = 60^\circ$, $\omega = 3.75$ and $\theta = 90^\circ$, $\omega = 2.55$. The maximum frequency for a spatial mode is the neutral-mode frequency, this amounts respectively for each polar angle: $\omega_N = 2.60$, 2.34 and 2.20 . For such a thickness of the heliopause, the solar rotation does not force any of its modes. Let us now consider a 10 AU thickness, we thus give in the Table II the forced spatial modes with their associated frequencies. Their wavelength is much smaller than the mixing-layer thickness. For $M_c = 0.51$, the forcing frequency is higher than the maximum permitted frequency. The thickness should be less than 7.28 AU to allow the heliopause at 30° for a forced mode. There hence exists a minimum polar angle above which heliopause modes can be forced. A maximum angle may also exist due to the heliopause thickness increase with θ and the neutral-mode frequency decrease with M_c . Perturbations along the heliopause therefore develop all the more rapidly so since the polar angle is far from both thresholds. After Fig. 15(b), for $M_c > 2$, $-\alpha_{i,ACT}$ starts to decrease. More generally, all growth rates decay with M_c , so we can assume that the amplification of these forced waves attains a maximum in the permitted θ -range. The maximum-growth disturbance is parallel to the heliopause for small \hat{M}_c . This is the case at $\theta = 60^\circ$ ($\hat{M}_c = 1.07$). On the contrary, if

\hat{M}_c becomes larger, the maximum-growth disturbance is oblique; at $\theta = 90^\circ$, $\hat{M}_c = 1.74$, the maximum amplification is given for an angle $\phi \simeq 23^\circ$ corresponding to the following values: $M_c \simeq 1.60$, $L \simeq 2.39 AU$, $L_e \simeq 5.47 AU$ and $\omega_r \simeq 1.40$. Such a e-folding length L_e is related to a variation of the polar angle of only 1.84° for a heliopause located at $170 AU$ from the Sun.

VII. SUMMARY AND CONCLUSIONS

The absolute/convective transition is given by the pinching of two first modes. The latter are two subsonic/subsonic vortex modes for small Mach numbers less than M_* and become two supersonic/subsonic vortex modes as $M \lesssim M_*$. The second modes which appear for $M \geq M_*$, subsonic/supersonic modes do not intervene in the transition because they propagate within the disturbance wavepacket with a higher real group velocity at any M . Although the spatial growth rate $-\alpha_i$ decreases with the Mach number, not only is the convective absolute transition still possible at high M , for $M > M_*$, but this passage occurs in fact earlier; the amount of backflow $-\beta_U$ required for taking the mixing layer toward absolute instability tends asymptotically to zero as M tends to infinity. The temporal growth rate in the absolute-instability zone nevertheless becomes very small for $M_c > 1$. The transition toward turbulence should become more difficult because slowed down by the appearance of intermediary basic flows, under the form of elongated Kelvin-Helmholtz billows. Fully developed turbulence is not really, however, completely reduced at high M ; Goebel and Dutton⁴⁶ found that transverse turbulence intensities and normalized kinematic Reynolds stresses decreased with increasing relative Mach number, whereas the streamwise turbulence intensities and kinematic Reynolds stress correlation coefficients remained relatively constant. Moreover as M_c increases, dispersion weakens. The absolute frequency of the ACT double root tends to zero at supersonic values. The group velocity also tends to zero. It is no longer therefore worth using notions of convective and absolute instabilities. The transition can be given with a very good approximation by the neutral slow mode as soon as the convective Mach number is supersonic. Besides, this study confirms Pavithran & Redekopp²⁴ and Jackson & Grosch²⁵'s studies undertaken at subsonic régime. Cooling the slow stream of a mixing layer has a destabilising effect whatever M may be. The baroclinic term in the vorticity transport equation, named baroclinic torque too, plays a prevailing rôle

in the passage to absolute instability. As we have recalled in the Introduction, it elongates the Kelvin-Helmholtz billows and causes the growth rate to decrease at high Mach number. Its action on the enhancement of the growth rate and on the acceleration of the passage to absolute instability is more efficient at low Mach numbers. Indeed, when the slow stream is very cooled, as soon as $\beta_T \lesssim 0.1$, a positive- β_U transition appears over a Mach number range that starts from $M \simeq 1$ and increases as β_T decreases. As $M < 1$, it is not possible to find damping unstable waves at very small β_T . The limit of existence of unstable waves is given by a third branch cut that had not been mentioned yet in the literature. The transonic state then becomes the most absolutely unstable. On the contrary, heating the slow stream can make the absolute instability vanish at low Mach numbers. The AC transition is as well all the earlier so since the temperature profile experiences a steep evolution within the mixing layer. At last, these numerical results do not only characterize the hyperbolic-tangent-like profile mixing layer but are qualitatively identical for any other mean profile that is decaying exponentially at infinity.

We have applied the results of the analysis to the stabilities of Interstellar Medium mixing layers and of the heliopause. Our main conclusions are the following ones. Using a ISM mixing layer model with a temperature ratio $\beta_T = 0.02$ corresponding to the smallest ratio that we could compute with our spectral method, we have deduced that the initial stage of the disturbance evolution was associated to a weakly absolutely unstable mixing layer. The KH mode that is excited has a small scale and a low temporal growth rate. The transition to turbulence is however given by a large-scale secondary instability.

The flanks of the heliopause defined by a polar angle $\theta \geq 30^\circ$ are characterized by a compressible plasma where the related Mach number increases gradually with θ . The flow is there convectively unstable. The periodic perturbation of the heliopause induced by the solar rotation forces this interface over a polar-angle range provided its thickness is sufficiently thin, roughly less than $17 AU$ in the $\theta \leq 90^\circ$ -range. The spatial growth rate can be then estimated fairly strong. Around $\theta = 90^\circ$ for example, this amplification corresponds to an arc less than 2° .

For a better relevance to space and astrophysical flows, we intend to introduce, for further papers, a magnetic field. After considering magnetohydrodynamic AC instability transition, Terra-Homem & Erdélyi⁴⁷ deduced that the presence of an external magnetic field had a strong stabilizing effect on the mixing-layer dynamics.

Acknowledgments

The author acknowledges the support of the PPARC/STFC (Particle Physics and Astronomy Research Council). He thanks Robertus Erdélyi and Michael Ruderman from the Department of Applied Mathematics of Sheffield University for helpful scientific and editing advice. He also thanks two anonymous referees for their constructing remarks.

-
- [1] W. D. Smyth, "Secondary Kelvin-Helmholtz instability in weakly stratified shear flow", *J. Fluid Mech.* **497**, 67-98(2003).
 - [2] P. Caillol, "Nonlinear internal waves in the upper atmosphere", *Geoph. Astroph. Fluid Dyn.* **99**, 4, 271-308(2005).
 - [3] M. C. Kelley, C. Y. Chen, R. R. Beland, R. Woodman, J. L. Chau and J. Werne, "Persistence of a Kelvin-Helmholtz instability complex in the upper troposphere", *J. Geoph. Res.* **110**, D14106, doi:10.1029/2004JD005345(2005).
 - [4] H. Hasegawa, M. Fujimoto, T.D. Phan, H. Rème, A. Balogh, M.W. Dunlop, C. Hashimoto and R. Tandokoro, "Transport of solar wind into Earth's magnetosphere through rolled-up MHD Kelvin-Helmholtz vortices", *Nature* **430**, 755-758(2004).
 - [5] M. E. Koepke and E. W. Reynolds, "Simultaneous, co-located parallel-flow shear and perpendicular-flow shear in low-temperature, ionospheric-plasma relevant laboratory plasma", *Plasma Phys. and Control. Fusion* **49**, 5A, A145-A157(2007).
 - [6] K. J. Mills, A. W. Longbottom, A. N. Wright, and M. S. Ruderman, "Kelvin-Helmholtz instability on the magnetospheric flanks: an absolute and convective instability approach", *J. Geoph. Res.* **105**, A12, 27685(2000).
 - [7] Y. Taroyan and R. Erdélyi, "Steady state excitation of field line resonances by global waveguide modes in the magnetosphere", *J. Geoph. Res.* **108**, A71301(2003).
 - [8] L. Landau, "Stability of tangential discontinuities in compressible fluid", *Doklady Akad. Nauk S.S.S.R., Proceedings* **44**, 139-141(1944).
 - [9] L. Lees and C. C. Lin, "Investigation of the stability of the laminar boundary layer in a compressible fluid", *NACA Technical Note* 1115(1946).
 - [10] W. O. Criminale, T. L. Jackson and R. D. Joslin, "Stability of compressible flows", in *Theory*

- and computation of hydrodynamic stability* (ed. Cambridge University Press, Cambridge, 2003), 132-172.
- [11] W. Blumen, "Shear layer instability of an inviscid compressible fluid", *J. Fluid Mech.* **40**, 4, 769-781(1970).
- [12] W. Blumen, P. G. Drazin and D. Billings, "Shear layer instability of an inviscid compressible fluid. Part II", *J. Fluid Mech.* **71**, 2, 305-316(1975).
- [13] P. G. Drazin and A. Davey, "Shear layer instability of an inviscid compressible fluid. Part III", *J. Fluid Mech.* **82**, 2, 255-260(1977).
- [14] S. A. Ragab and J. L. Wu, "Linear instabilities in two-dimensional compressible mixing layers", *Phys. Fluids A* **1**, 6, 957-966(1989).
- [15] T. L. Jackson and C. E. Grosch, "Inviscid spatial stability of a compressible mixing layer", *J. Fluid Mech.* **208**, 609-637(1989).
- [16] L. M. Mack, "On the inviscid acoustic-mode instability of supersonic shear flows Part 1: two-dimensional waves", *Theoret. Comput. Fluid Dynamics.* **2**, 97-123(1990).
- [17] N. D. Sandham and W. C. Reynolds, "Compressible mixing layer: linear theory and direct simulation", *AIAA J.* **28**, 4, 618-624(1990).
- [18] D. Papamoschou, "Communication paths in the compressible shear layer", *AIAA Pap.* 90-0155, *AIAA 28th Aerospace Sciences Meeting, Reno, Nevada*(1990).
- [19] P. J. Lu and K. C. Wu, "Numerical investigation on the structure of a confined supersonic mixing layer", *Phys. Fluids A* **3**, 12, 3063-3079(1991).
- [20] S. A. Ragab and S. Sheen, "The nonlinear development of supersonic instability waves in a mixing layer", *Phys. Fluids* **4**, 3, 553-566(1992).
- [21] P. Huerre and P. A. Monkewitz, "Absolute and convective instabilities in free shear layers", *J. Fluid Mech.* **159**, 151-168(1985).
- [22] D. J. Forliti, B. A. Tang and P. J. Strykowski, "An experimental investigation of planar counter-current turbulent shear layers", *J. Fluid Mech.* **530**, 241-264(2005).
- [23] B. J. Bayly, S. A. Orszag and T. Herbert, "Instability mechanisms in shear-flow transition", *Ann. Rev. Fluid Mech.* **20**, 359-391(1988).
- [24] S. Pavithran and L. G. Redekopp, "The absolute-convective transition in subsonic mixing layers", *Phys. Fluid A* **1**, 10, 1736-1739(1989).
- [25] T. L. Jackson and C. E. Grosch, "Absolute/convective instabilities and the convective Mach

- number in a compressible mixing layer”, Phys. Fluids **2**, 6, 949-954(1990).
- [26] M. Terra-Homem and R. Erdélyi, “Absolute and convective instabilities in open shear layers, part I Hydrodynamic equilibrium”, Astro. and Astrophy. **403**, 425-432(2003).
- [27] V. D. Djordjevic and L. G. Redekopp, “Linear stability analysis of nonhomentropic, inviscid compressible flows”, Phys. Fluids **31**, 11, 3239-3245(1988).
- [28] L. Brevdo, “Initial-boundary-value stability problem for the Blasius boundary layer”, Z. angew. Math. Mech. **75**, 5, 371-378(1995).
- [29] G. Chimonas, “The extension of the Miles-Howard theorem to compressible fluids”, J. Fluid Mech. **43**, 833-836(1970).
- [30] S. Le Dizès, P. Monkewitz and P. Huerre, “Viscous structure of plane waves in spatially developing shear flows”, Phys. Fluids **7**, 6, 1337-1347(1995).
- [31] R. Peyret, “Chebyshev method”, in *Spectral methods for incompressible viscous flow* (ed. by Springer, 2002), 39-100.
- [32] T. J. Bridges and P. J. Morris, “Differential eigenvalue problems in which the parameter appears nonlinearly”, J. of Comp. Phys. **55**, 437-460(1984).
- [33] P. Caillol and M. Ruderman, “Absolute and convective instabilities in an inviscid compressible mixing layer”, Astro. Notes (Astronomische Nachrichten) **328**, 8, 747-751(2007).
- [34] T. L. Jackson and C. E. Grosch, “ Inviscid spatial stability of a compressible mixing layer Part 3. Effect of thermodynamics”, J. Fluid Mech. **224**, 159-175(1991).
- [35] C. Olendraru, A. Sellier, M. Rossi and P. Huerre, “Inviscid instability of the Batchelor vortex: Absolute-convective transition and spatial branches”, Phys. Fluids **11**, 7, 1805-1820(1999).
- [36] P. Meliga, D. Sipp and J-M. Chomaz, ”Absolute instability in axisymmetric wakes: compressible and density variation effects”, J. Fluid Mech. **600**, 373-401(2008).
- [37] M. M. Rogers and R. D. Moser, “The three-dimensional evolution of a plane mixing layer: the KH rollup”, J. Fluid Mech. **243**, 183-226(1992).
- [38] H. Goertler , “Berechnung von aufgaben der freien turbulenz auf grund eines neuen na-herungsansatzes”, ZAMM **22**, 244-254(1942).
- [39] N. Lardjane, I. Fedioum and I. Gökalp, “Accurate initial conditions for the direct numerical simulation of temporal compressible binary shear layers with high-density ratio”, Comput. and Fluids **33**, 4, 549-576(2004).
- [40] M. C. Begelman and A. C. Fabian, ”Turbulent mixing layers in the interstellar and intracluster

- medium”, *Month. Notices of the Roy. Astro. Soc.***244**, 2, P26-P29(1990).
- [41] A. Esquivel, R. A. Benjamin, A. Lazarian, J. Cho, and S. Leitner, “Magnetohydrodynamic turbulent mixing layers: Equilibrium cooling models”, *Astroph. J.***648**, 2, 1043-1051(2006).
- [42] H.J. Fahr, W. Neutsch, S. Grzedzielski, W. Macek, R. Ratkiewicz-Landowska, “Plasma transport across the heliopause”, *Space Sci. Rev.***43**, 329-381(1986).
- [43] V. B. Baranov, “Gasdynamics of the solar wind interaction with the interstellar medium”, *Space Sci. Rev.***52**, 89-120(1990).
- [44] V. Izmodenov, Y. Malama and M. S. Ruderman, “Solar cycle influence on the interaction of the solar wind with Local Interstellar Cloud”, *Astron. & Astrophys.***429**, 1069-1080(2005).
- [45] V. B. Baranov, M. G. Lebedev and M. S. Ruderman, “Structure of the region of solar wind-interstellar medium interaction and its influence on H atoms penetrating the solar wind”, *Astrophys. and Space Sc.***66**, 441-451(1979).
- [46] S. G. Goebel and J. C. Dutton, “Experimental-study of compressible turbulent mixing layers”, *AIAA J.***29**, 4, 538-546(1991).
- [47] M. Terra-Homem and R. Erdélyi, “Absolute and convective instabilities in open shear layers, part II Magnetohydrodynamic equilibrium”, *Astro. and Astrophys.***413**, 7-15(2004).

V_{hot} (km/s)	M_c	instability	wavelength L (pc)	growth rate	growth scale τ (kyear), L_e (pc)
120	1	AU	6.79	$\omega_i \sim 0.045$	$\tau \sim 90$
170	1.30	AU	0.82	$\omega_i \sim 0.047$	$\tau \sim 61$
204	1.49	AU	0.085	$\omega_i \sim 0.025$	$\tau \sim 96$
240	1.75	ACT	0.068	$\omega_i \sim 0, -\alpha_i \sim 11.73$	$\tau \sim \infty, L_e \sim 0.043$
300	2.19	CU	0.270	$-\alpha_{i,\text{max}} = 6.10$	$L_e = 0.082$

TABLE I: Instabilities in a ISM mixing-layer model: $\beta_U = 0$ and 1 pc-wide protonic-gas mixing layer.

θ	β_T	ϕ	M_c	frequency ω_r	wavelength L (AU)	growth rate $-\alpha_i$	e-folding length L_e (AU)
30°	0.019	0	0.51	$3.57 > \omega_N$	—	—	—
60°	0.021	0	1.07	1.87	1.72	0.679	7.36
		30°	0.93	2.16	1.47	0.321	15.58
90°	0.021	0	1.74	1.28	2.62	0.877	5.70
		30°	1.51	1.47	2.24	0.905	5.52
		45°	1.23	1.80	1.79	0.709	7.05

TABLE II: Convective instabilities along a heliopause model: $\beta_U = 0.081$ and 10 AU-wide protonic-gas mixing layer.

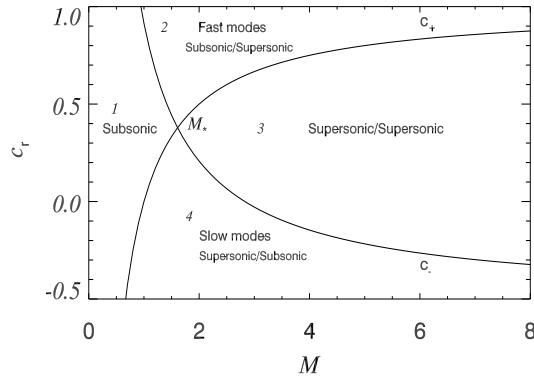
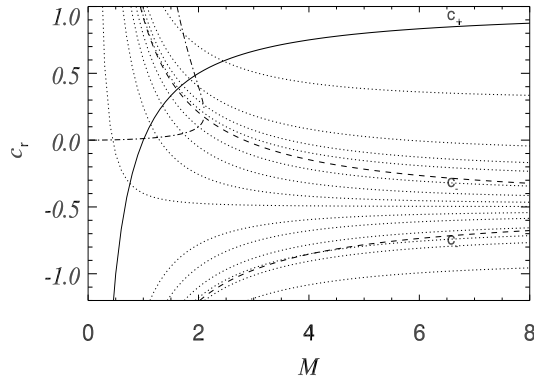
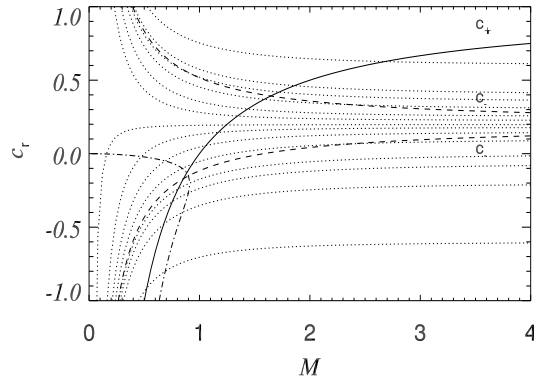


FIG. 1: Branch cuts c_{\pm} versus Mach number for $\beta_U = -0.5$ and $\beta_T = 2$.

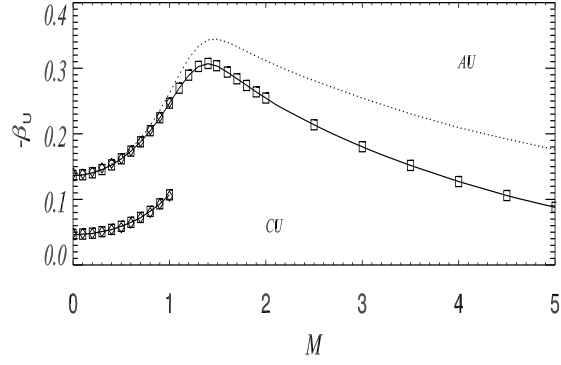


(a)

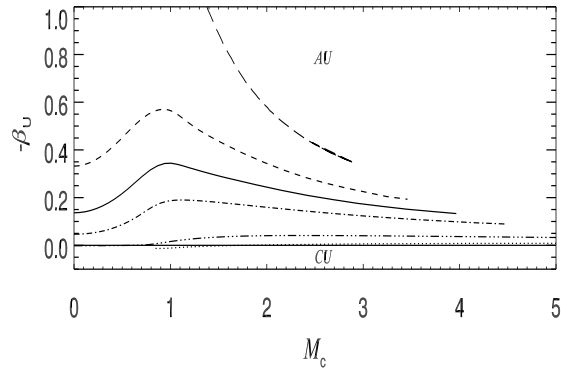


(b)

FIG. 2: Branch cuts at $c_i = 0.2$: (a) $\beta_T = 2$, $\beta_U = -0.5$; (b) $\beta_T = 0.1$, $\beta_U = 0.2$; dotted line branch cuts $c_{2,-,r}^{\pm}$ at $-\alpha_i/\alpha_r = 0.12, 0.25, 0.75, 1, 2, 4, 10$ and 100 , for $\beta_U < 0$ and the opposite for $\beta_U > 0$, dot-dashed line, branch cut $c_{2,-,r}$ for which $\omega_i = 0$ from Eq. 14.



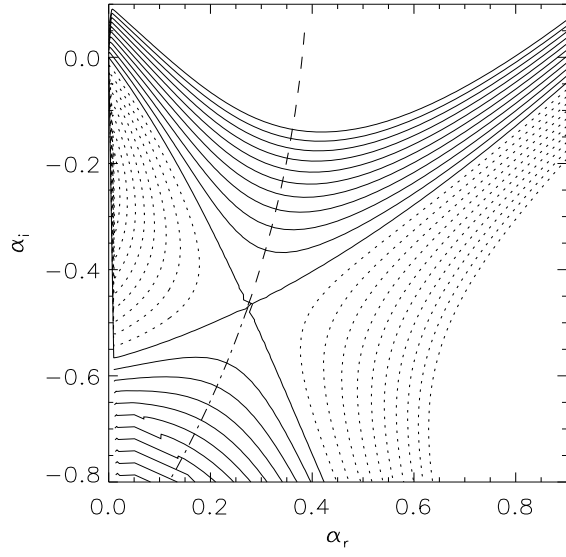
(a)



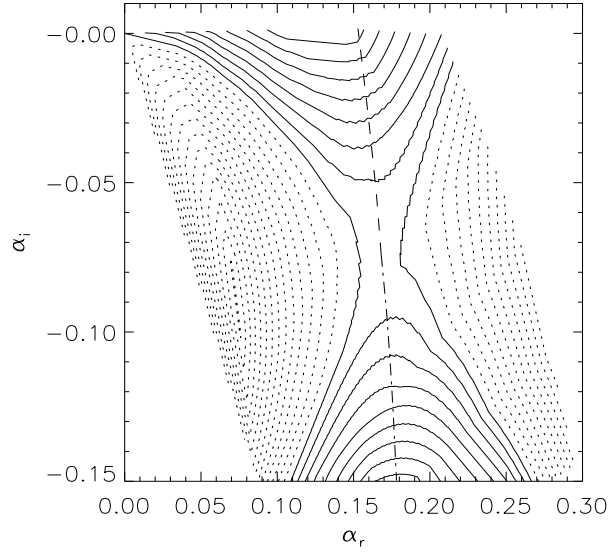
(b)

FIG. 3: (a) Comparison between different computations of the ACT modes in the (β_U, M) plane: \diamond from Jackson and Grosch²⁵, \square from Runge-Kutta scheme integration of (5), solid lines from the spectral method with the temperature profile (3), $\beta_T = 0.5$ and $\beta_T = 1$, dotted line $\beta_T = 1$ and temperature profile (2). *AU* stands for absolutely unstable and *CU* for convectively unstable.

(b) ACT modes in the (β_U, M_c) plane for various values of β_T . The legend stands for: dotted line $\beta_T = 0.02$, three-dot-dashed line $\beta_T = 0.1$, dot-dashed line $\beta_T = 0.5$, solid line $\beta_T = 1$, short dashed line $\beta_T = 2$, long dashed line $\beta_T = 10$.

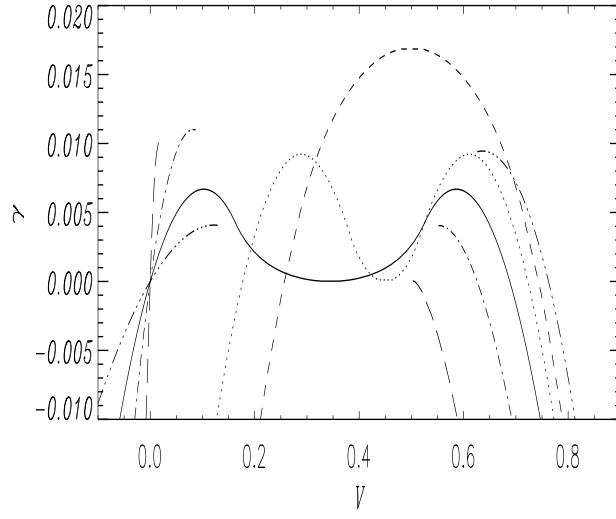


(a)

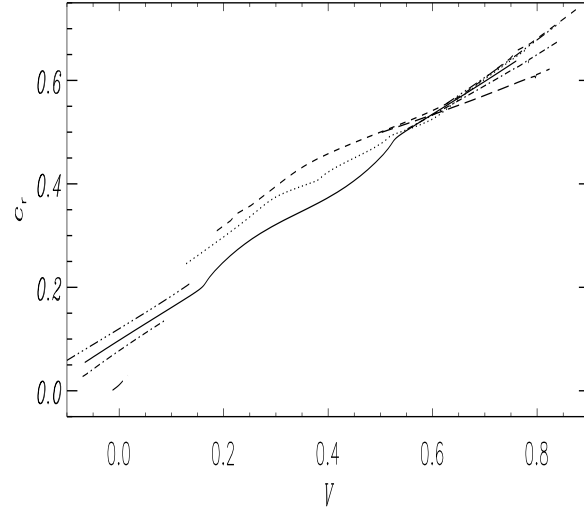


(b)

FIG. 4: Contours of ω_i in the α -plane for two ACT modes at $\beta_T = 1$: (a) $\beta_U = -0.1641$ and $M = 0.5$, (b) $\beta_U = -0.2541$ and $M = 3$. Long-dashed and dot-dashed lines are the two branches $\omega_r = \omega_{0,r}$, one is upstream and the second downstream showing the pinching condition.

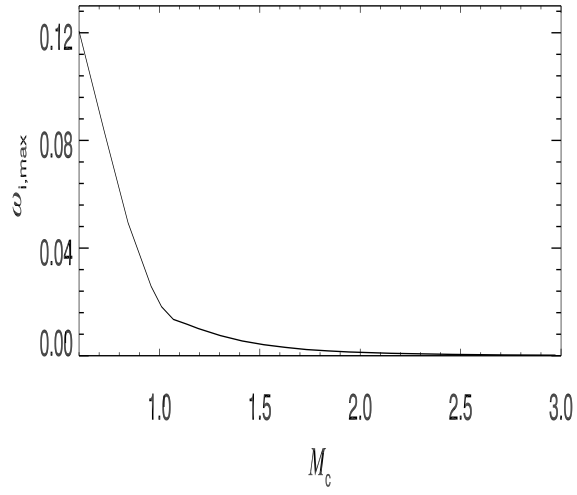


(a)

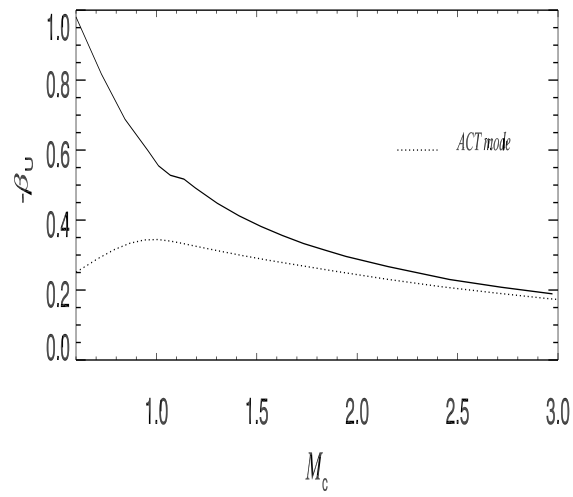


(b)

FIG. 5: (a) Growth rate $\gamma = \omega_i - \alpha_i V$ and (b) phase speed c_r , as functions of V at $M = 2$. $\beta_T = 1$: solid line $\beta_U = -0.3116$, dotted line $\beta_U = -0.1$ and dashed line $\beta_U = 0$; $\beta_T = 0.5$: dot-dashed line $\beta_U = -0.1840$; $\beta_T = 2$: three-dot-dashed line $\beta_U = -0.4985$; $\beta_T = 0.02$: long-dashed line $\beta_U = 13.5 \cdot 10^{-6}$; γ has been divided by 10 for the slow-mode growth of that last value of β_T .

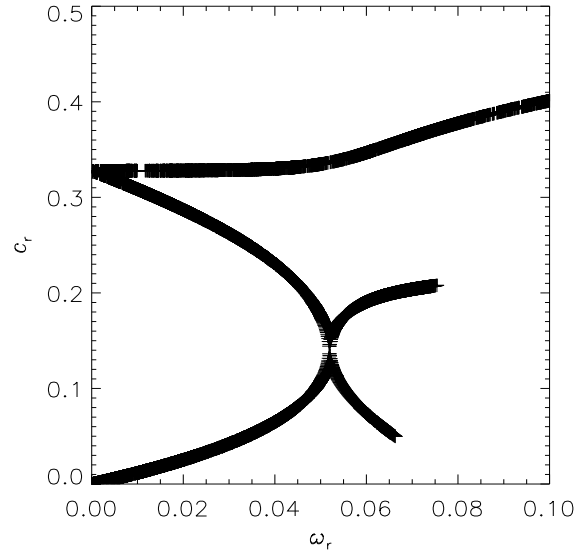


(a)

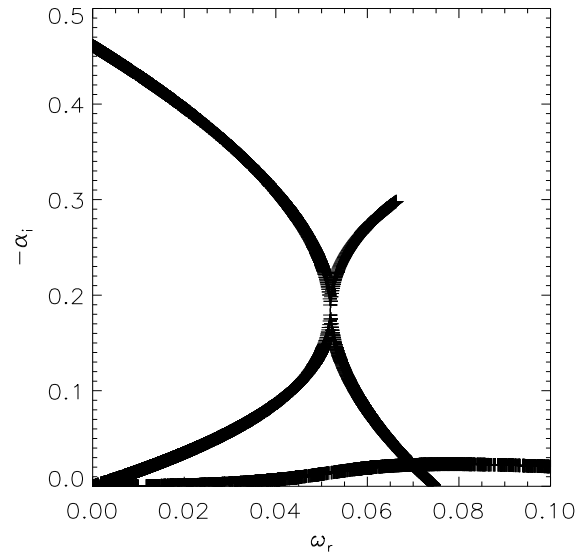


(b)

FIG. 6: The double root possessing the maximum ω_i for $\beta_T = 1$ (solid line): (a) ω_i and (b) $-\beta_U$ as functions of M_c .

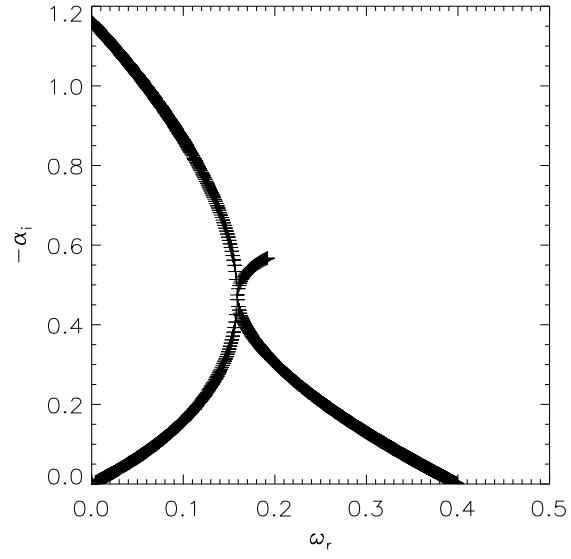


(a)

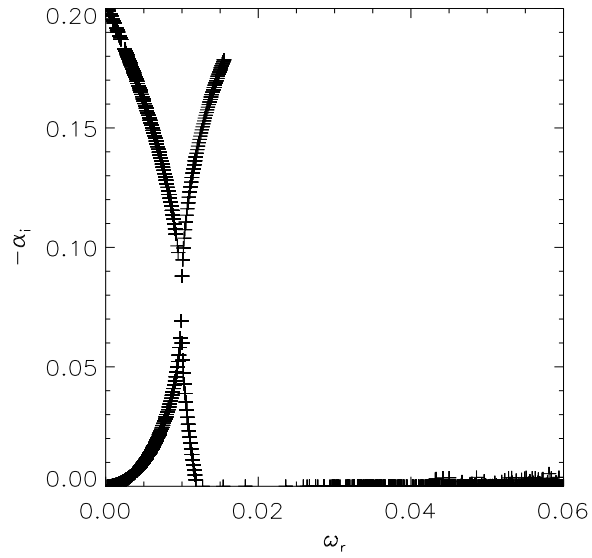


(b)

FIG. 7: The first and second modes $\beta_U = -0.3443$, $\beta_T = 1$, $M = 1.5$ ($M_c \simeq 1.01$), ACT mode $c_r = 0.1403$, $\alpha_r = 0.2012$, $\alpha_i = -0.1844$ and $\omega_r = 0.519$: (a) c_r and (b) $-\alpha_i$ as functions of ω_r .



(a)



(b)

FIG. 8: The spatial growth rate $-\alpha_i$ as a function of ω_r at $\beta_T = 1$ for the first and second modes: (a) $\beta_U = -0.1641$, $M = 0.5$ ($M_c \simeq 0.29$), $\alpha_r = 0.2737$, $\alpha_i = -0.4690$, $c_r = 0.1475$ and $\omega_r = 0.1589$, and (b) $\beta_U = -0.2541$, $M = 3$ ($M_c \simeq 1.88$), $\alpha_r = 0.1684$, $\alpha_i = -0.0735$ and $\omega_r = 0.0099$.

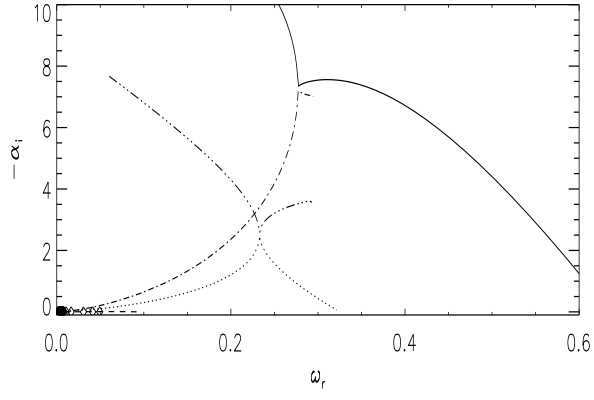
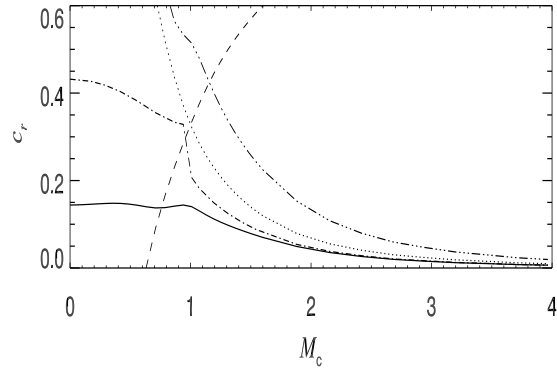
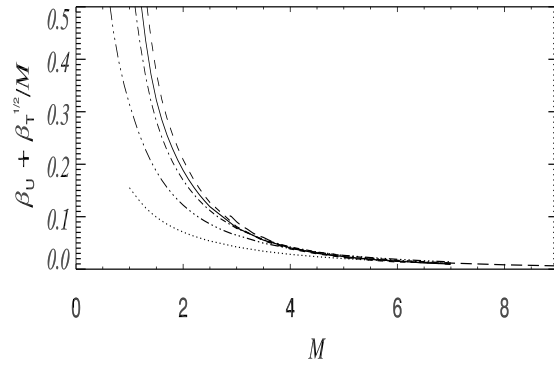


FIG. 9: Pinching ACT double roots at $M = 1.4$: $\beta_T = 0.1$, $\beta_U = -0.0206$ ($M_c = 1.09$), and $\beta_T = 0.02$, $\beta_U = 0.0064$ ($M_c \sim 1.22$); α_1^+ : dotted line and dot-dashed line, α_1^- : three-dot dashed line and solid line, α_2^+ : dashed line ($\beta_T = 0.1$) and \diamond ($\beta_T = 0.02$).

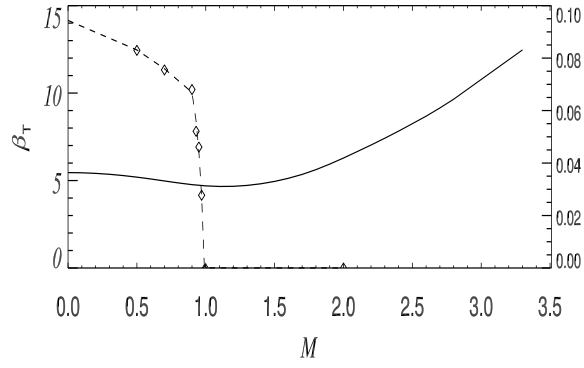


(a)

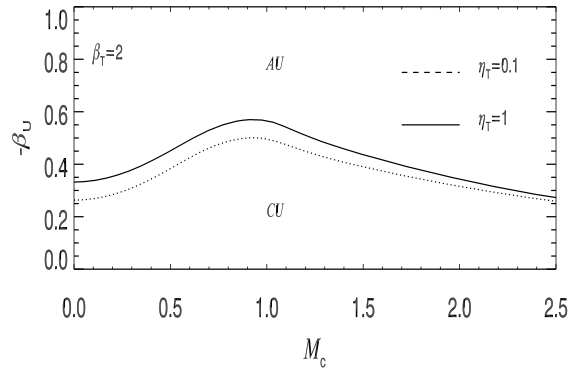


(b)

FIG. 10: (a) ACT-mode phase speed (solid line) with the branch cuts c_+ (dashed line), c_- (dotted line), $c_{2,-,r}$ (three-dot-dashed line) given respectively by (9), (11) and (14), and the neutral-mode phase speed (dot-dashed line) for $\beta_T = 1$; (b) asymptotic behaviour of ACT β_U at high Mach numbers, same legend as in Fig. 3 (b).



(a)



(b)

FIG. 11: (a) Limiting values of ACT β_T as a function of M ; maximum value for a counterflow $\beta_U = -1$, solid line, and minimum value at the edge of the branch cut from Eq. 14, numerical data dashed line, β_T given by Eq. 14 \diamond , with the corresponding scale on the right axis, (b) $-\beta_U$ as a function of M_c at $\beta_T = 2$.

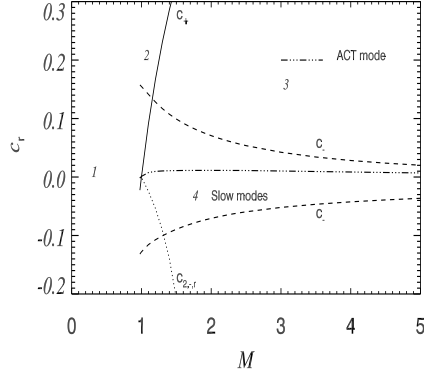
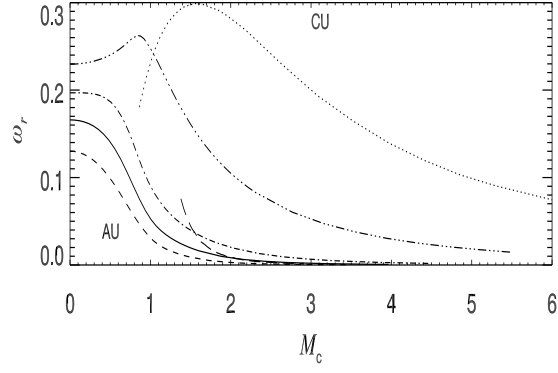
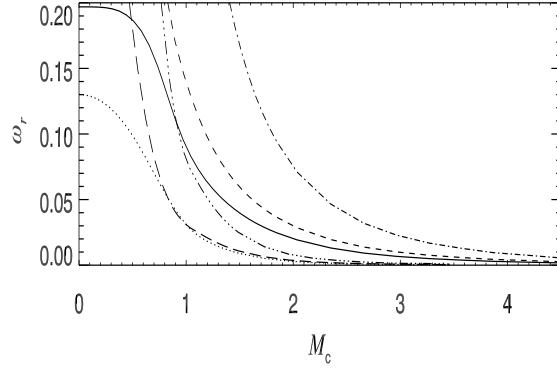


FIG. 12: Branch cuts in the (c_r, M) plane for $\beta_T = 0.02$, $c_-: \beta_U \pm \beta_T^{1/2}/M$, the curve $c_{2,-,r}$ is determined by taking Eq. 14 and using α_{ACT} and $\beta_{U,ACT}$, $b^2 > 0$ in Eq. 13 for $M \leq 0.99$. The first double root appears at $M = 0.978$ for $c_r \simeq -0.0020$, $c_{2,-,r} \simeq -0.0016$, it is a subsonic mode located in the domain 1. As soon as $M \gtrsim 1$, ($M_c \gtrsim 0.888$), ACT modes belong to the domain 4.

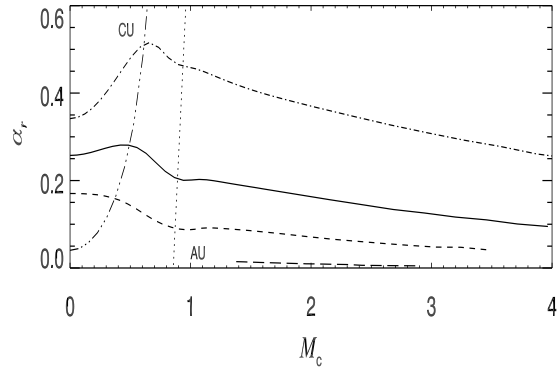


(a)

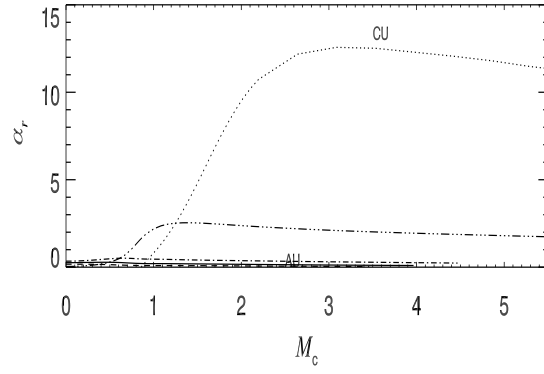


(b)

FIG. 13: (a) ACT modes in the (ω_r, M_c) plane for various values of β_T ; for $\beta_T = 10$, ω_r has been magnified by a factor 50, same legend as in Fig. 3 (b); (b) ACT absolute frequencies with their branch cuts (14); $\beta_T = 0.5$: solid line ω_r ; dashed line $\alpha_r c_-$; dot-dashed line ω_2^- ; $\beta_T = 2$: dotted line ω_r , long-dashed line $\alpha_r c^-$, three-dot-dashed line ω_2^- .



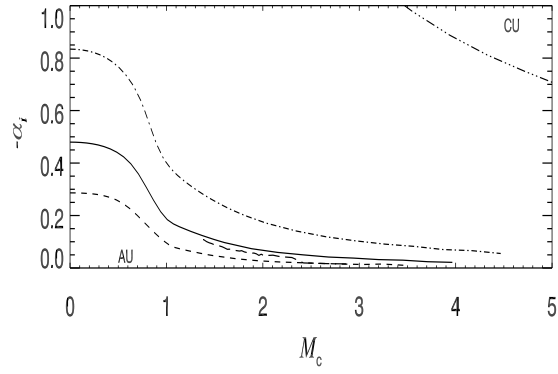
(a)



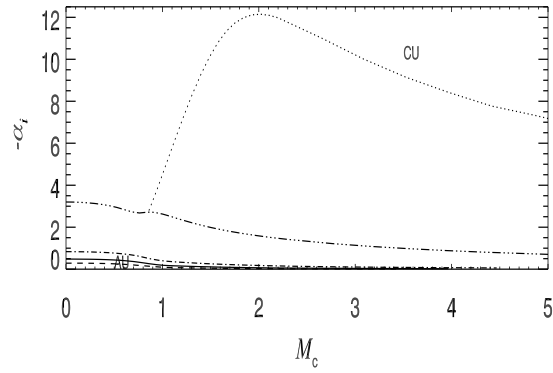
(b)

FIG. 14: ACT modes in the (α_r, M_c) plane for various values of β_T , same legend as in Fig. 3 (b).

(a) zoom at small α_r .

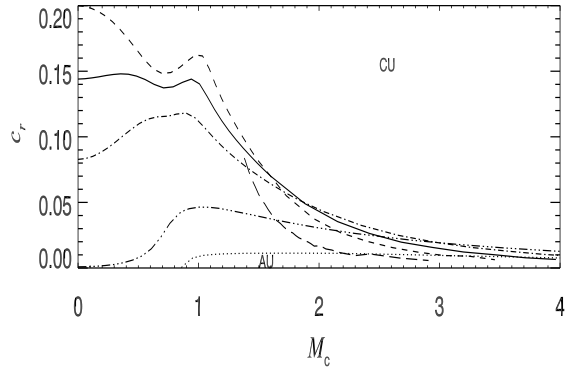


(a)

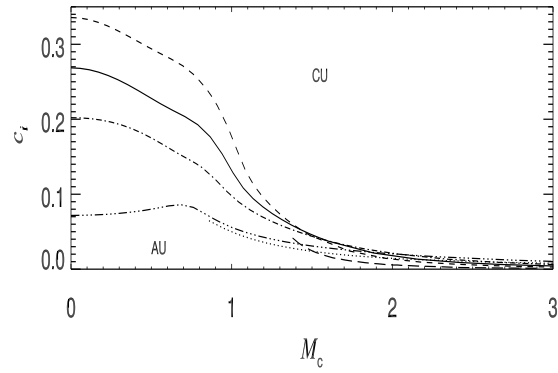


(b)

FIG. 15: ACT modes in the (α_i, M_c) plane for various values of β_T , same legend as in Fig. 3 (b). The spatial growth rate has been magnified by 15 for the case $\beta_T = 10$. (a) zoom at small $-\alpha_i$.

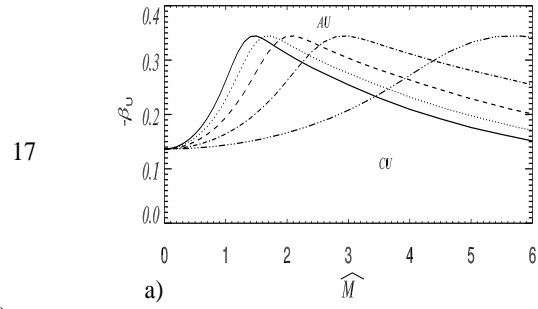


(a)

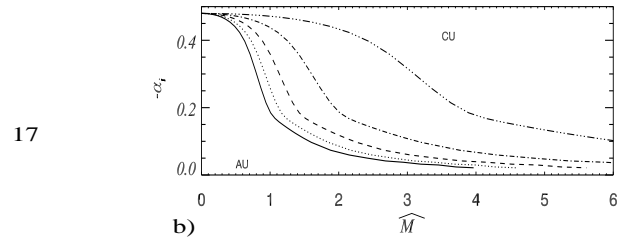


(b)

FIG. 16: ACT modes in (a) the (c_r, M_c) plane and in (b) the (c_i, M_c) plane for various values of β_T , same legend as in Fig. 3 (b).

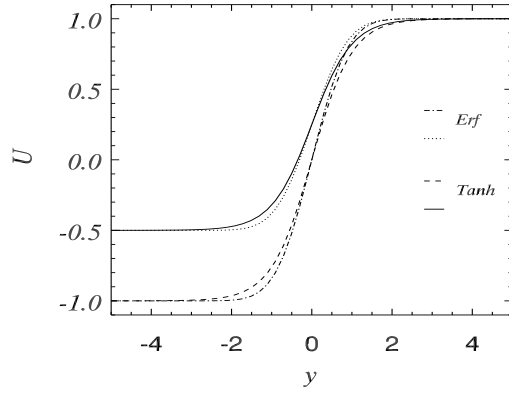


(a)

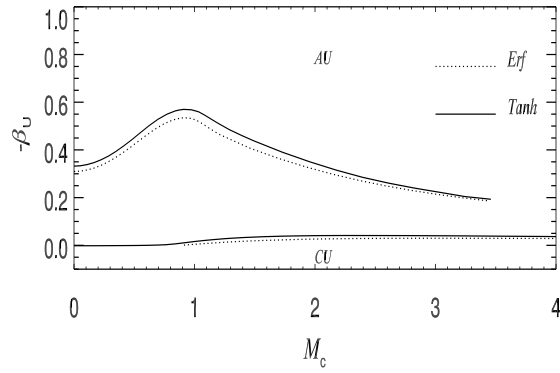


(b)

FIG. 17: Effect of the angle ϕ as a function of $\hat{M} = M/\cos\phi$ at $\beta_T = 1$ on (a) the ACT ratio β_U and on (b) the spatial instability $-\alpha_i$. Solid line $\phi = 0^\circ$, dotted line $\phi = 30^\circ$, short-dashed line $\phi = 45^\circ$, dot-dashed line $\phi = 60^\circ$ and three-dot-dashed line $\phi = 75^\circ$.



(a)



(b)

FIG. 18: Comparison of Tanh and Erf-like U profiles with $\text{erf}[\eta] = 2/\pi^{1/2} \int_0^\eta e^{-t^2} dt$: a) profiles $U(y)$ at $\beta_U = -0.5$ and $\beta_U = -1$; b) $-\beta_U$ as a function of M_c at $\beta_T = 0.1$ and $\beta_T = 2$.

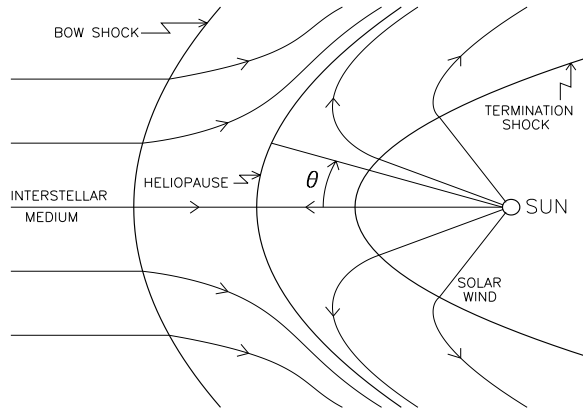


FIG. 19: Schematic of the heliosphere